

Hawaii National Marine Renewable Energy Center (HINMREC)

U.S. Department of Energy Award Number:
DE-FG36-08GO18180

Task 5: Wave Energy Conversion Device Performance

WEC Ocean Testing: Testing Support, Progress Report 1

Prepared by:
DNV GL Energy

Prepared for:
Hawaii Natural Energy Institute, University of Hawaii

April 2016



HAWAII NATIONAL MARINE RENEWABLE ENERGY CENTER – WEC
OCEAN TESTING

Testing Support – Progress Report #1

Hawaii Natural Energy Institute (HNEI)

Report No.: 702053-USSD-T-04, Rev. B

Date: 25 April 2016



IMPORTANT NOTICE AND DISCLAIMER

1. This document is intended for the sole use of the Client as detailed on the front page of this document to whom the document is addressed and who has entered into a written agreement with the DNV GL entity issuing this document ("DNV GL"). To the extent permitted by law, neither DNV GL nor any group company (the "Group") assumes any responsibility whether in contract, tort including without limitation negligence, or otherwise howsoever, to third parties (being persons other than the Client), and no company in the Group other than DNV GL shall be liable for any loss or damage whatsoever suffered by virtue of any act, omission or default (whether arising by negligence or otherwise) by DNV GL, the Group or any of its or their servants, subcontractors or agents. This document must be read in its entirety and is subject to any assumptions and qualifications expressed therein as well as in any other relevant communications in connection with it. This document may contain detailed technical data which is intended for use only by persons possessing requisite expertise in its subject matter.
2. This document is protected by copyright and may only be reproduced and circulated in accordance with the Document Classification and associated conditions stipulated or referred to in this document and/or in DNV GL's written agreement with the Client. No part of this document may be disclosed in any public offering memorandum, prospectus or stock exchange listing, circular or announcement without the express and prior written consent of DNV GL. A Document Classification permitting the Client to redistribute this document shall not thereby imply that DNV GL has any liability to any recipient other than the Client.
3. This document has been produced from information relating to dates and periods referred to in this document. This document does not imply that any information is not subject to change. Except and to the extent that checking or verification of information or data is expressly agreed within the written scope of its services, DNV GL shall not be responsible in any way in connection with erroneous information or data provided to it by the Client or any third party, or for the effects of any such erroneous information or data whether or not contained or referred to in this document.
4. Any wind or energy forecasts estimates or predictions are subject to factors not all of which are within the scope of the probability and uncertainties contained or referred to in this document and nothing in this document guarantees any particular wind speed or energy output.

KEY TO DOCUMENT CLASSIFICATION

Strictly Confidential	:	For disclosure only to named individuals within the Client's organisation.
Private and Confidential	:	For disclosure only to individuals directly concerned with the subject matter of the document within the Client's organisation.
Commercial in Confidence	:	Not to be disclosed outside the Client's organisation.
DNV GL only	:	Not to be disclosed to non-DNV GL staff
Client's Discretion	:	Distribution for information only at the discretion of the Client (subject to the above Important Notice and Disclaimer and the terms of DNV GL's written agreement with the Client).
Published	:	Available for information only to the general public (subject to the above Important Notice and Disclaimer).

Project name:	Hawaii National Marine Renewable Energy Center – WEC Ocean Testing	DNV GL Energy Renewables Advisory Americas 9665 Chesapeake Drive Suite 435 San Diego CA 92123 USA Tel: +1 858 836 3370 Registered in America No. 94- 3402236
Report title:	Testing Support – Progress Report #1	
Customer:	Hawaii Natural Energy Institute (HNEI)	
Contact person:	Luis Vega	
Date of issue:	25 April 2016	
Project No.:	702053	
Report No.:	702053-USSD-T-04, Rev. B	

Prepared by:	Verified by:	Approved by:
<hr/> Steve Parkinson Engineer, Wave & Tidal Energy	<hr/> Ben Child Technical Lead, Wave & Tidal Energy	<hr/> Ricard Buils Urbano Head of Wave & Tidal Head of Loads Analysis
<hr/>	<hr/>	
<hr/>	<hr/>	

<input type="checkbox"/> Strictly Confidential <input type="checkbox"/> Private and Confidential <input type="checkbox"/> Commercial in Confidence <input type="checkbox"/> DNV GL only <input checked="" type="checkbox"/> Client's Discretion <input type="checkbox"/> Published	Keywords: Performance, Loading, Verification
---	--

Reference to part of this report which may lead to misinterpretation is not permissible.

Rev. No.	Date	Reason for Issue	Prepared by	Verified by	Approved by
A	29/02/2016	First issue	S Parkinson	B Child	R Buils Urbano
B	20/04/2016	Re-issue following comments	S Parkinson	B Child	R Buils Urbano



Table of contents

1	INTRODUCTION	2
2	ENVIRONMENTAL CONDITIONS AT THE WETS SITE	4
3	MODEL SETUP AND OUTPUTS	12
4	RESULTS	16
4.1	Regular waves	16
4.2	Unidirectional irregular sea states	20
4.3	Irregular spread waves	29
4.4	Extreme response analysis	35
5	CONCLUSIONS	43
6	REFERENCES	44

Appendices

APPENDIX A WAVEDYN OUTPUT FILES	45
---------------------------------------	----



1 INTRODUCTION

This technical note is issued to the Research Corporation of the University of Hawaii (RCUH or the "Client") pursuant to a written Agreement for Services effective 14 March 2013 and RCUH Purchase Order #Z10027978 /1/ as well as the subsequent amendment to the agreement /2/. The Client has requested that Garrad Hassan America, Inc. (DNV GL) perform services relating to the establishment of a wave energy test center for the University of Hawaii, Hawaii Natural Energy Institute (UH HNEI). UH HNEI's Hawaii National Marine Renewable Energy Center (HINMREC), under funding from the U.S. Department of Energy (DOE) is working in collaboration with the U.S. Navy to develop the Wave Energy Test Site (WETS or the "Project") located at U.S. Marine Corps Base Hawaii – Kaneohe (MCBH-K) in Oahu, Hawaii.

The project consists of three main components /1/:

1. Documentation of test protocols and support to the testing program
2. Provision of data for verification of Wave Energy Converter (WEC) performance models
3. Provision of data for verification of WEC array models

The present technical note forms part of the *second* project component.

As per the service agreement /1/, the scope of the second component of the project is to use DNV GL's in-house WEC performance and loading analysis tool WaveDyn to assist with the verification of HNEI's WEC performance model. WaveDyn has been subjected to a range of validation exercises and was developed specifically for WECs. The tool allows for flexible, multi-body modelling of a wide range of WEC concepts in time domain simulations and couples loading from critical areas including hydrodynamics, power take off, and moorings.


Initially it was intended that HNEI would supply outputs from their own performance models for a series of real WEC devices being tested at the WETS site and DNV GL would generate independent models and simulations for comparison. However, due to the lack of availability of data relating to the devices being tested at WETS and following discussion with HNEI, it has been agreed /5/ that DNV GL will instead simulate a range of *generic* WEC models in conditions representative of the WETS site in order to provide a database of results for later use by HNEI.

An advantage of basing this work on a range of generic WEC devices is that the definition of each model can be chosen to clearly demonstrate a variety of physical phenomena that are important to capture by any numerical model. Also, the chosen models can be based on other previous physical or numerical validation work, which is beneficial for cross-referencing of results.

Furthermore, it is has been agreed between DNV GL and HNEI /5/ that the technical support to the testing programme detailed in /1/ under deliverables 5.1 and 5.2 would most usefully take the form of providing further verification data for HNEI's numerical models. This will allow increased confidence in the numerical predictions generated by HNEI and thus enhance understanding of the data relating to the WECs that are installed at WETS.

Therefore, the present phase of work (provision of data for verification of WEC performance models) will be associated with five deliverables:

1. WEC performance model verification progress report #1
2. Testing support progress report #1
3. WEC performance model verification progress report #2

- 
4. Testing support progress report #2
 5. WEC performance model verification final report

A previous technical note /7/ (which refers to the first deliverable above) described investigations into the most appropriate scale at the WETS site for the first generic WEC model; a *rounded cylinder single-body point absorber*. Indicative performance and capital expenditure costs (CAPEX) were derived for different device sizes of the same geometry. Following review of this information and taking into account practical considerations, HNEI have decided to pursue a 20 m diameter WEC in 60 m water depth (corresponding to one of the berths at WETS) /6/ for the remainder of the verification exercises. This is equivalent to a scale of 1:40 using the 0.5 m diameter numerical model of the buoy.

The present technical note refers to the *second* deliverable for this phase and documents the progress that has been made on the analysis of the rounded cylinder single-body point absorber. Detailed performance and loading results are presented relating to the aforementioned WEC geometry and using the selected scale and water depth. All numerical simulations were performed at model scale and the results interpreted in this technical note at full scale using Froude Scaling laws. Flow solver inputs have been updated for the simulations described in this technical note to reflect the newly-defined ratio between water depth and buoy diameter. Where possible, results have been derived for a wide a range of environmental conditions (a subset of which would be representative of the WETS site), although in some instances (e.g. for extremes) conditions are based on site-specific data.

Section 2 describes the derivation of the extreme environmental conditions at the WETS site to be used in the subsequent detailed analysis. In Section 3, the updates to the numerical model described in /7/ necessary for this work are described, before the corresponding results in normal operational and extreme sea states are given in Section 4. Finally, some concluding remarks are given in Section 5. All input and output files will be supplied to HNEI to facilitate further verification exercises (via an agreed medium).

2 ENVIRONMENTAL CONDITIONS AT THE WETS SITE

In order to describe the wave environmental conditions at the WETS site, a combination of measured buoy data and numerical hindcast data has been used. The hindcast data was obtained from an existing study /8/ while the buoy data was obtained from the National Data Buoy Centre (NDBC) . The location and duration of the data sets used to describe the temporal variation of the wave resource are given in Figure 2-1 and Table 2-1.

The data has been processed to provide both normal operational and extreme wave conditions. The data sets and analysis methodology for the normal and extreme wave conditions are discussed in more detail in Sections 2.1.1 and Section 2.1.2 respectively.

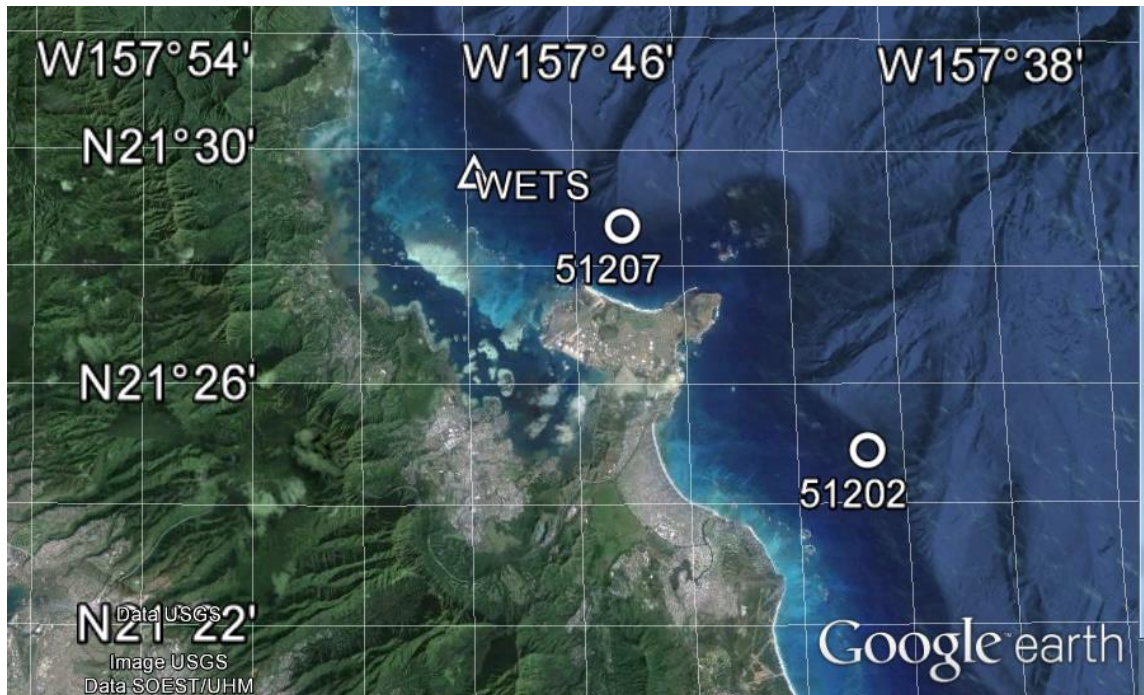


Figure 2-1 Oahu Island and location of the Wave Energy Test Site (WETS) denoted by triangle. Location of buoy data sets 51207 and 51202 used to derive extreme wave climate are denoted by circles. Wave hindcast information is provided at the same location as 51207.

Table 2-1 Summary of data sets used to characterise normal operational and extreme site conditions

Data	Coverage [dd/mm/yyyy]	Water depth [m]	Latitude	Longitude
Kane'oha Bay Buoy 51207(198)	26/10/2012- 21/10/2015	81	21°28'39"N	157°45'9"W
Mokapu Point Buoy 51202(098)	09/08/2000- 12/10/2015	89	21°24'54"N	157°40'41"W
Numerical Hindcast	1979-2013	80	21°28'39"N	157°45'7"W

2.1.1 Normal operational conditions

A set of simulations has been performed associated with normal operational conditions (i.e. it is assumed that the machine will be producing power). For these simulations, a variety of irregular sea states have been considered. A number of regular wave conditions have also been considered to illustrate the behaviour of the WEC more clearly. The following sea states have therefore been used in the simulations (the mean wave direction of all simulation was 0 deg):

1. **Case I - Regular** sea states with wave amplitude a and wave period T defined using the following combinations have been simulated:

- a. Wave amplitudes $a = 0.4, 0.8, 1.2, 2, 3, 4$ m
- b. Wave periods $T = 1.58, 3.16, 4.74, 5.60, 5.7, 6.32$, and then every 0.316 s to 25.3 s.
- c. The (mean) direction of waves is along the x -axis ($MDIR = 0$).

Only combinations of height and period that do not exceed the breaking wave steepness limit have been simulated. For deep water the wave breaking limit, given by the wave height to wave length ratio otherwise known as the wave steepness ϵ , occurs at $\epsilon = 1/7$ [12]. The wave steepness for deep water waves can be written $\epsilon = 4\pi a/gT^2$ where g is the acceleration due to gravity.

2. **Case II - Unidirectional and irregular** sea states defined using the following range of significant wave height $H_s = 0.5, 1.0, \dots, 5.5$ m and energy period $T_e = 5, 6, \dots, 17$ s and the following additional specification:

- a. The frequency-dependent wave spectra (omnidirectional spectra) are described using a JONSWAP spectral shape with a peak enhancement factor $\gamma = 1$. The JONSWAP spectral shape is given by:

$$S_j(f) = \frac{\alpha g^2}{(2\pi)^4 f} \exp\left(-\frac{5}{4}\left(\frac{f_p}{f}\right)^4\right) \gamma^r \quad (1)$$

$$r = \exp\left(-\frac{(f - f_p)^2}{2\sigma_j^2 f}\right) \quad (2)$$

$$\sigma_j = \begin{cases} 0.07, & f < f_p \\ 0.09, & f \geq f_p \end{cases} \quad (3)$$

where, f is the wave frequency, α is the energy scale, $f_p = 1/T_p$ is the peak frequency and σ_j is the peak-width parameter. The peak period T_p of the JONSWAP spectra is obtained using the fixed ratio between energy period and peak period $T_p = 1.17 T_e$.

It was decided that a JONSWAP spectrum would be used as a representation of the wave climate for each sea state. In this way, results from this study can be applied to other sites (also assuming a JONSWAP spectral shape) by accounting for the site-specific distribution of wave height and period.

- b. The mean wave direction is along the x -axis, $MDIR = 0$.
- c. The same seed (initialising the random phases of wave components) was used for all simulations.
- d. The simulation duration was set at 3 hours.

3. **Case III - Directional spread and irregular** sea states defined as per case II and the following additional specification:

- a. Omnidirectional wave spectra were described using a JONSWAP spectral shape with a peak enhancement factor of $\gamma=1$.
- b. The mean wave direction is along the x -axis, $MDIR = 0$.
- c. The directional distribution is described using a Ewans wind sea distribution /13/. The wave direction is denoted by θ . For unimodal sea states the direction distribution $D(\theta, f)$ is based on the wrapped normal distribution given by:

$$D(\theta, f) = \frac{1}{\sigma(f)\sqrt{2\pi}} \sum_{k=-\infty}^{\infty} \exp\left(-\frac{1}{2}\left(\frac{\theta - MDIR - 2\pi k}{\sigma(f)}\right)^2\right) \quad (4)$$

$$\sigma = \begin{cases} 11.38 + 5.357\left(\frac{f}{f_p}\right)^{-7.929}, & f < f_p \\ 32.13 - 15.39\left(\frac{f}{f_p}\right)^{-2}, & f \geq f_p \end{cases} \quad (5)$$

For the Ewans wind sea, the standard deviation is described empirically and is frequency dependent.

Information regarding the directional spread of waves was not provided as part of this work. Equation (4) and (5) were applied as they provided a means of describing the directional distribution in the absence of other information. While the Ewans wind sea is theoretically specific to wind generated waves, a similar formulation can be used to describe swell waves using a different formula for σ . However, in DNV GL's experience, the Ewans wind sea representation of directional distribution offers a good description of directional spread for both wind and swell seas.

- d. The same seed (initialising the random phases of wave components) was used for all simulations.
- e. The simulation duration was set at 30 minutes.

The range of H_s and T_e values have been derived from the WETS scatter table of $H_s - T_e$ which has been obtained from a metocean hindcast /8/ conducted by the Department of Ocean and Resources Engineering at the University of Hawaii. The hindcast provides a time series of H_s and T_e around the WETS site for a 34 year period. A validation study was conducted as part of the hindcast study /8/ using measurements collected using NDBC buoy data.

The hindcast outputs also include the wave spectra which could be used for WaveDyn simulations. Instead a JONSWAP spectra has been used in simulations as this will make the results suitably generic such that model verification can also be conducted for other sites.

The time series data used to define the normal wave conditions was obtained from /8/ at a point coincident with Buoy 51207 at Kane'oha bay. The scatter table of H_s and T_e at the WETS site is presented in Table 2-2 and Figure 2-2. Figure 2-2 shows the scatter table of occurrence of H_s and T_e at the WETS site. A line of constant significant steepness of 0.07 has been added to the scatter table. Above this threshold sea states are not realistic as wave-breaking would prevent these sea states from occurring in reality. The significant steepness is defined as:

$$S_e = \frac{2\pi H_s}{g T_e^2} \quad (6)$$

It can be seen that all states at the WETS site lie below a line of constant significant steepness of 0.07. When processing the results of simulations for Case II and III the significant steepness will be used to exclude simulations of that do not satisfy the criteria $S_e < 0.07$.

Table 2-2 Scatter table of occurrence of H_s and T_e at the WETS site (probability density is in % x10)

Hs [m]	Te [s]												
	5	6	7	8	9	10	11	12	13	14	15	16	17
0.5	0.05	0.80	1.34	1.24	0.41	0.09	0.08	0.02	0.00	0.00	0.00	0.00	0.00
1	3.66	36.18	45.46	36.38	25.17	15.21	7.66	2.38	0.89	0.30	0.02	0.00	0.00
1.5	1.19	100.95	125.02	69.41	48.35	31.64	21.66	8.80	3.43	1.21	0.32	0.05	0.00
2	0.00	19.94	97.34	52.81	32.56	20.49	13.91	8.56	4.01	1.55	0.76	0.18	0.02
2.5	0.00	0.19	26.90	29.66	14.60	10.07	6.87	4.83	2.48	1.35	0.49	0.17	0.02
3	0.00	0.00	3.05	17.86	7.15	4.85	3.13	2.78	1.21	0.62	0.33	0.06	0.01
3.5	0.00	0.00	0.02	4.71	4.06	1.50	1.06	0.71	0.46	0.25	0.06	0.04	0.00
4	0.00	0.00	0.00	0.69	2.35	0.53	0.38	0.42	0.18	0.22	0.16	0.02	0.00
4.5	0.00	0.00	0.00	0.02	0.78	0.29	0.13	0.14	0.19	0.00	0.00	0.00	0.00
5	0.00	0.00	0.00	0.00	0.18	0.16	0.01	0.00	0.04	0.00	0.00	0.00	0.00
5.5	0.00	0.00	0.00	0.00	0.00	0.08	0.00	0.00	0.00	0.01	0.00	0.00	0.00

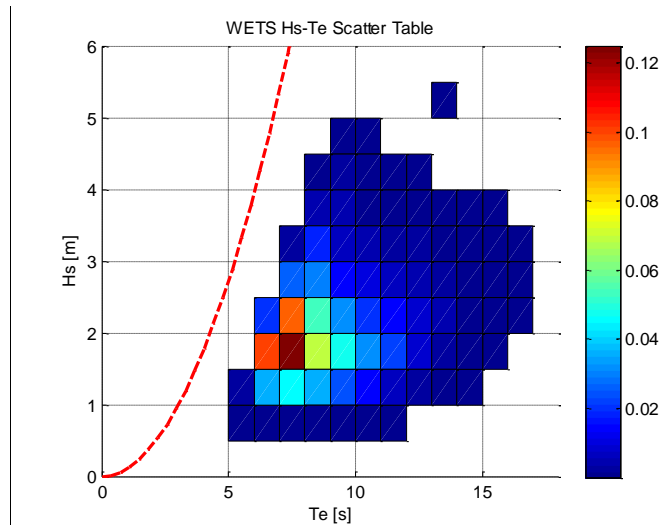


Figure 2-2 Probability density for H_s and T_e describing wave conditions at WETS site. Colorbar denotes the probability density. Red dashed line corresponds to constant significant steepness of 0.07.

2.1.2 Extreme conditions

For the simulations of extremes, the following cases have been considered:

1. **Case IV - Unidirectional and irregular** sea states defined using extreme return values for significant wave height with 1, 5, 10, 50 and 100 year return periods and associated energy period and the following additional specification:
 - a. Omnidirectional wave spectra were described using a JONSWAP spectral shape with a peak enhancement factor of $\gamma=1$ as given in Equation (1).
 - b. The mean wave direction is along the x -axis, $MDIR = 0$.
 - c. The same seed was used for all simulations.
 - d. The simulation duration was set at 3 hours.
2. **Case V - Directional spread and irregular** sea states defined using extreme return values for significant wave height with 1, 5, 10, 50 and 100 year return periods and associated energy period and the following additional specification:
 - a. Omnidirectional wave spectra were described using a JONSWAP spectral shape with a peak enhancement factor of $\gamma=1$.
 - b. The mean wave direction is along the x -axis, $MDIR = 0$.
 - c. The directional distribution is described using a Ewans wind sea distribution as described in Equations (4) and (5).
 - d. The same seed (initialising the random phases of wave components) was used for all simulations.
 - e. The simulation duration was set at 30 minutes.

2.1.2.1 Extreme significant wave height

The return values for significant wave height are derived via analysis of on-site measurement data collected using buoys. The NDBC buoy data collected at the site is summarised in Table 2-1. Buoy 51207 is the closest to the test site; however, the corresponding data record is only 3 years in duration. Buoy 51202 is nearby and has a record length close to 15 years, which is more suitable for the evaluation of extremes. In Figure 2-3, a comparison of H_s shows that the buoy data sets 51207 and 51202 are highly correlated. The return values of H_s at WETS are therefore estimated using buoy 51202, on the basis that the estimated H_s between the two buoys are in good agreement and no calibration is required. This is confirmed by examination of the regression plot and Q-Q plot in Figure 2-3.

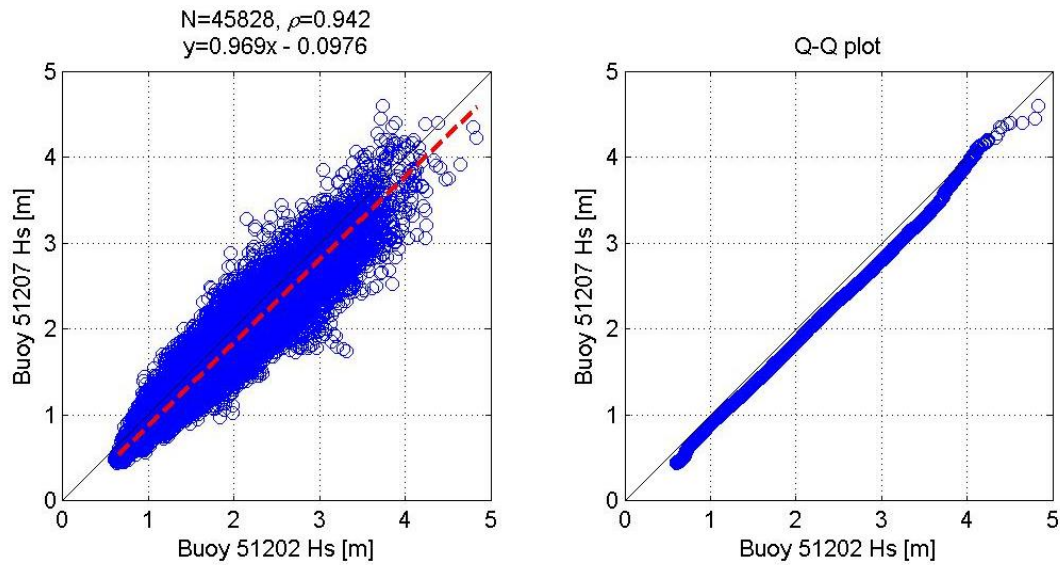


Figure 2-3 Regression plot (right) and Q-Q plot (left) of H_s recorded at buoy 51207 and 51202.

The extreme wave conditions have been calculated using the buoy 51202 data. The extreme H_s has been calculated using a peaks-over-threshold (POT) method as described in /10/. The analysis is carried out as follows:-

- The time series is 'declustered' to select only the largest H_s within a window of 48 hours.
- A threshold is selected by fitting the Generalised Pareto Distribution (GPD) to the declustered data for a range of thresholds and checking for convergence to a steady state value of the GPD shape parameter and steady estimates of high quantiles. The threshold is then selected as the lowest level for which convergence is achieved.
- The GPD is fitted to the data point that are above the selected threshold level.
- The fitted distribution is used to calculate return values at return periods of 1, 5, 10, 50, and 100 years.

The extremes analysis has been conducted using all the data (an omnidirectional) analysis. The GPD fit (Figure 2-4) is checked by defining empirical non-exceedence probabilities as follows /10/:

$$P_i = \frac{i - 0.35}{N} \quad (7)$$

Good agreement is found between the model and the observations. The return levels are summarised in Table 2-3.

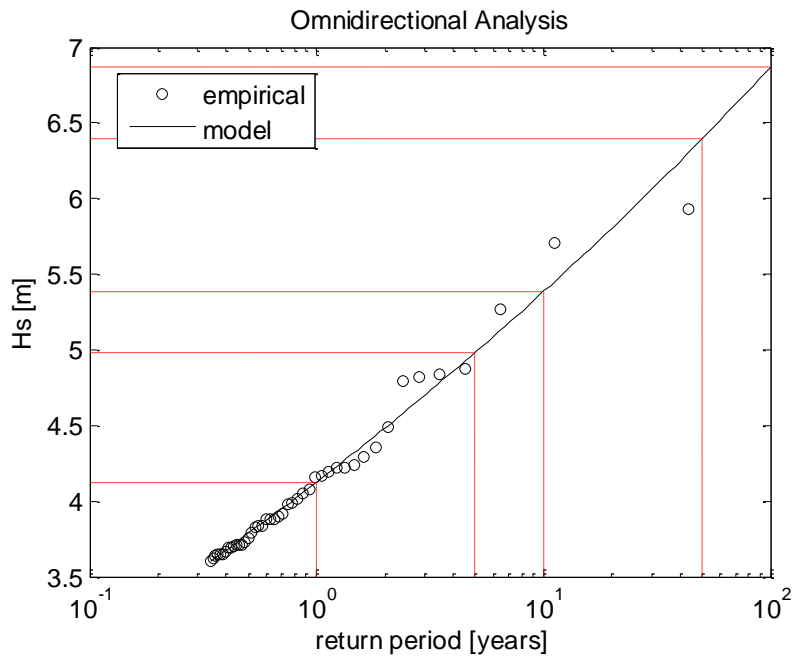


Figure 2-4 GPD fit to observations of extreme wave height observed at buoy 51202. Red dashed lines denote return levels.

Table 2-3 Summary of return levels for H_s and associated energy period T_e

Return Period [year(s)]	1	5	10	50	100
Hs [m]	4.13	4.98	5.38	6.40	6.87
Associated energy period					
Te LB [s]	8.0	8.8	9.1	9.9	10.3
Te mean [s]	9.6	10.6	11.0	12.0	12.4
Te UB [s]	15.8	17.3	18.0	19.6	20.3

2.1.2.2 Associated return period

A range of values for the associated wave energy period have been estimated using the significant steepness and return values for H_s . Figure 2-5 shows the significant steepness computed using the data collected by buoy 51202. The minimum, mean and maximum significant steepness value per H_s is evaluated and then these curves are used to calculate the associated energy period by re-arranging Equation (6) to obtain:

$$T_{assoc} = \sqrt{2\pi \frac{H}{gS_e}} \quad (8)$$

Equation (8) is evaluated using the min, mean, max significant steepness to obtain an upper bound, mean and lower bound energy period. For $H_s > 4$ m there is insufficient data to infer min, max and mean values of S_e with great confidence. Therefore the significant steepness at $H_s = 4$ m is used to calculate the associated wave period for all return values.

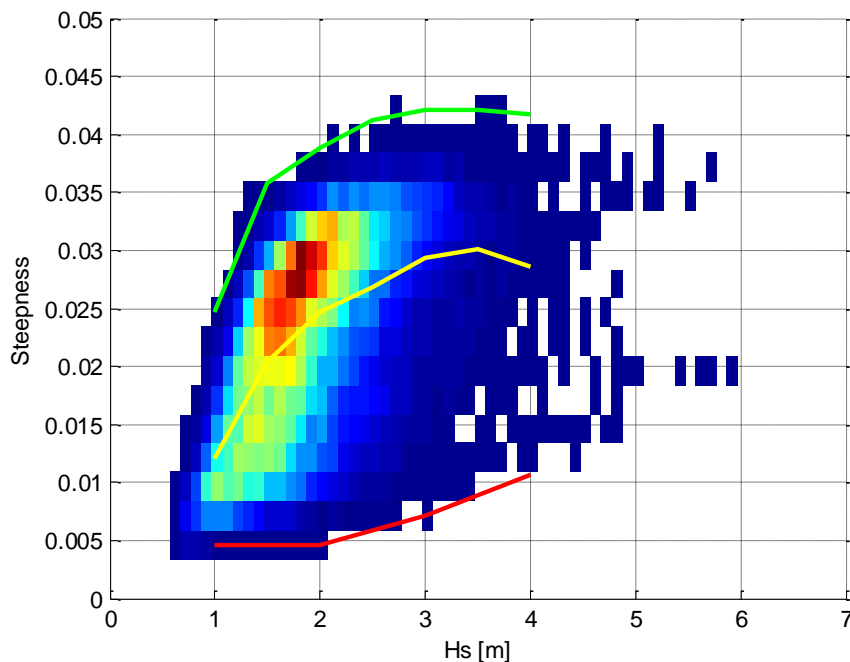


Figure 2-5 Significant wave steepness against significant wave height for Buoy 51202. Colour denotes probability density. The green and red lines show upper and lower bounds to significant steepness and the yellow line gives mean wave steepness with respect to H_s .

3 MODEL SETUP AND OUTPUTS

The simulations in this report have been conducted using a point absorber-type WEC with dimensions based on a model-scale test device. The point absorber model used in the numerical simulations is identical to that described in /7/, except for the changes described in this section. The original model scale point absorber is of 0.5 m diameter and was simulated in a water depth of 2.8 m in /7/. Following the study in /7/ where the optimal ratio between diameter and water depth was investigated, it was agreed with HNEI that, at full-scale, a 20 m diameter point absorber should be simulated for a WETS berth with a water depth of 60 m. This results in a diameter to water depth ratio of 1:3. The model has been modified to satisfy this ratio so that the simulations accurately predict performance and loads at the WETS site.

The WEC model used for numerical simulations in the present study is depicted in Figure 3-1 and Figure 3-2. A summary of the main parameters of the WEC model is provided in Table 3-1. The WEC model is the same as in /7/, except for the following changes:

1. The water depth in the model scale WEC definition (WaveDyn) file has been changed to 1.5 m.
2. The lengths of structural components of the WEC in the WaveDyn file were reduced by 1.3 m to maintain the same buoy draught. Rigid link 1 defined in the WaveDyn model /7/ was reduced by 0.78 m and Rigid link 2 by 0.52 m.
3. The flow solver (WAMIT) simulations were re-run to update the hydrodynamic coefficients for the new 1:3 diameter to depth ratio.
4. Additional degrees of freedom were added to the hinge joints in the WaveDyn file to enable roll of the device as well as pitch during the simulation of spread seas. Figure 3-2 provides a schematic of the point absorbers multi-body representation in the simulation tool WaveDyn.

All simulations were conducted at model scale. However, the outputs have been reported as full-scale values using the Froude scale rules set out in /7/. The ratio between lengths in the new point absorber numerical model and the desired 'full-scale' device is 1:40 and so a scale factor of $k=40$ is used to transform outputs from model to 'full-scale'.

Note that none of the simulations took into account viscous forces, which are difficult to characterise accurately and add to a linear hydrodynamic model. When modelling energetic and extreme conditions viscous forces are likely to become important. However, results are presented here using the pure linear hydrodynamic formulation so that verification exercises with equivalent formulations may be easily performed and so that the difference in results when more detailed approaches are used is more apparent.

The following model outputs, that are used to describe the WEC response to extreme and normal operational conditions, are as follows:

1. The 'Buoy-ST-Kinematics' (i.e. the motions of the buoy in global space):
 - a. Global Surge ϕ_x
 - b. Global Sway ϕ_y
 - c. Global Heave ϕ_z
 - d. Global Roll ϕ_{Rx}
 - e. Global Pitch ϕ_{Ry}

2. The 'Total System Power Take-Off (PTO) Performance' (i.e. power-related variables):
 - a. PTO Power Output ϕ_p
3. The 'Spring-By-Freedom-PTO' (i.e. tether-related variables):
 - a. Joint Freedom Displacements ϕ_d
 - b. Applied Force ϕ_F

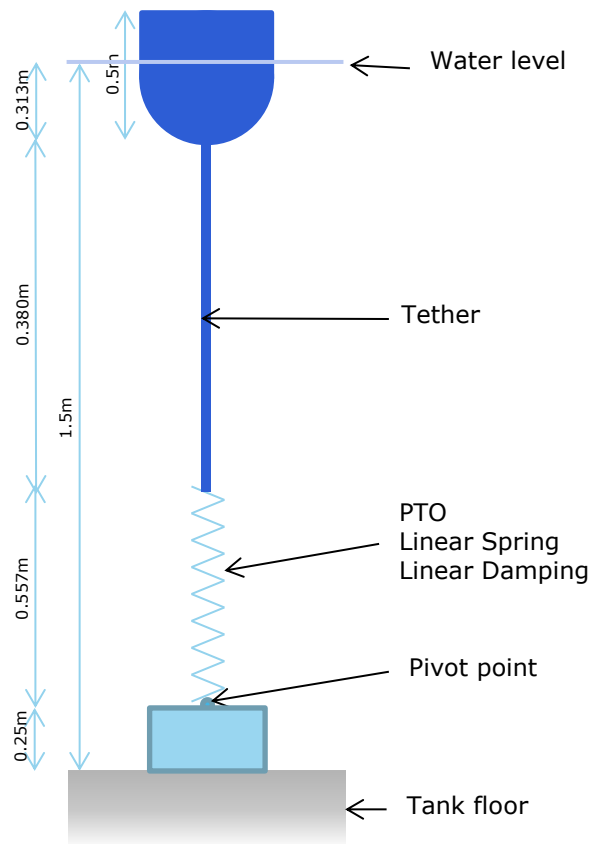


Figure 3-1 Schematic diagram of the generic WEC device moored to the tank floor.

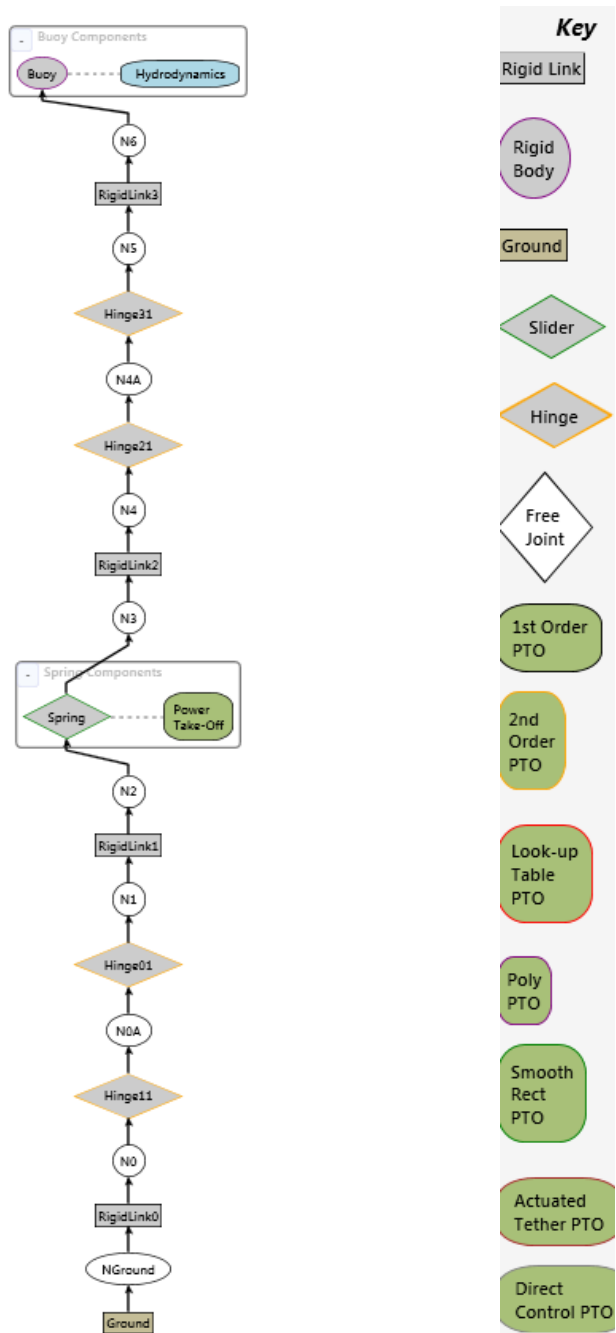


Figure 3-2 WaveDyn model schematic.

Table 3-1 Main parameters describing the point absorber

Parameter	Model scale	Full-scale
Buoy definition		
Water depth [m]	1.5	60
Buoy draft [m]	0.313	12.52
Diameter [m]	0.5	20
Buoy Mass [kg]	43.2	2.76×10^6
PTO definition		
Damping [Ns/m]	37.7	3.81×10^5
Stiffness [N/m]	66.3	1.06×10^5
Pre-load [N]	35.8	4.59×10^5

4 RESULTS

Time domain simulations of the WEC model described in Section 3 have been conducted in the WaveDyn tool. The environmental conditions described in Section 2 have been used to describe the normal operational and extreme wave conditions. The following results are presented here:

1. Section 4.1 shows the response amplitude operators, force amplitude operators and relative capture width derived from simulations of regular waves.
2. Sections 4.2 and 4.3 provide the minimum, maximum, and root mean squared (RMS) variation of buoy kinematics, and PTO forces and power output for normal operational conditions.
3. Time series of peak loads during extreme simulations are provided in Section 4.4.

4.1 Regular waves

A series of simulations in regular waves were conducted in order to compute the response amplitude operators (RAO) for the buoy kinematics, the relative capture width of the point absorber and the force amplitude operator (FAO) on the PTO. A range of regular wave periods and amplitudes were used to conduct simulations as described in Section 2.1.1 (Case I).

The response and force amplitude operators are calculated using the following equation for the amplitude of response or force:

$$X = \sqrt{2} \cdot SD[\hat{\phi}_i - \langle \hat{\phi}_i \rangle] \quad (9)$$

where $\hat{\phi}_i$ is a time history of the point absorber motions and forces for $i = x, y, z, Rx, Ry, d$ where all frequencies except the fundamental frequency have been removed from the signal. The signal processing, includes curtailing the simulation ramp-up time and calculating the moving mean of the signal, where the window is equal to the regular wave period. The time series is curtailed to a duration of 25 times the wave period. This curtailed time series is taken from the end of the time series to ensure that transients in motions and forces are not included. The operators SD and $\langle \cdot \rangle$ are the standard deviation and mean of the time series output. Once the response and force amplitude are computed, the response or force amplitude operator is then given by X/a .

For each wave amplitude and period the significant steepness was computed using Equation (6). An upper limit to the wave steepness ϵ of 1/7 was imposed as discussed in Section 2.1.1. All results under the wave breaking limit are included in the analysis.

The RAOs of the buoy heave are calculated using the ϕ_z kinematics of the buoy and the results are shown in Figure 4-1. It can be seen from the invariant RAOs that the global buoy heave is overwhelmingly linear with respect to wave amplitude (as expected from the linearity of the hydrodynamics and structural constraints in this degree of freedom). In addition, there is a resonance in the heave motion of the buoy close to an angular frequency of 0.9 rad/s, which corresponds to a 7 s wave period. At low angular frequencies or long wave periods (>7 s), the model tends to follow the incident wave elevation and so the RAO tends to unity. In contrast, for short period waves (<5 s) the buoy does not respond significantly to incident wave excitation. These features of the response are entirely expected for wave energy devices and in particular point absorbers.

The surge and pitch RAOs are derived from the ϕ_x and ϕ_β motions of the buoy and are presented in Figure 4-2 and Figure 4-3 respectively. These plots reveal a second resonance in the system just under 0.8 rad/s corresponding to approximately an 8 s wave period. It is noted that this resonance is in the pitching motion but it also affects the surge motion due to the structural coupling in the WEC. The global

buoy pitch response is reasonably linear but the RAO is not the same around the resonant angular frequency for all incident wave amplitudes indicating nonlinearities in the machine response. The RAO for surge also indicates a long period resonance which is associated with rotation around the anchor point. This nonlinearity is due to the geometric nonlinearities in the model, with the two hinge joints placed below and above the PTO resulting in coupling between the pitch and surge motions.

The force amplitude operator has been computed using the PTO applied force. The result shows that the greatest loading occurs due to incident waves with a period of approximately 6 to 8 s.

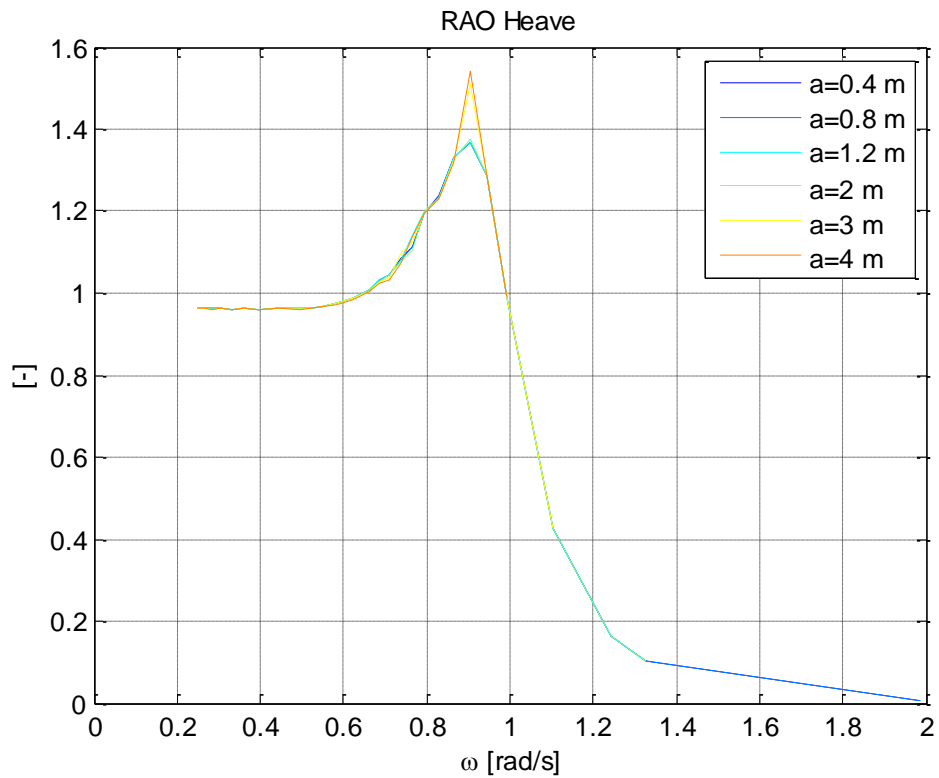


Figure 4-1 Response amplitude operator of buoy global heave

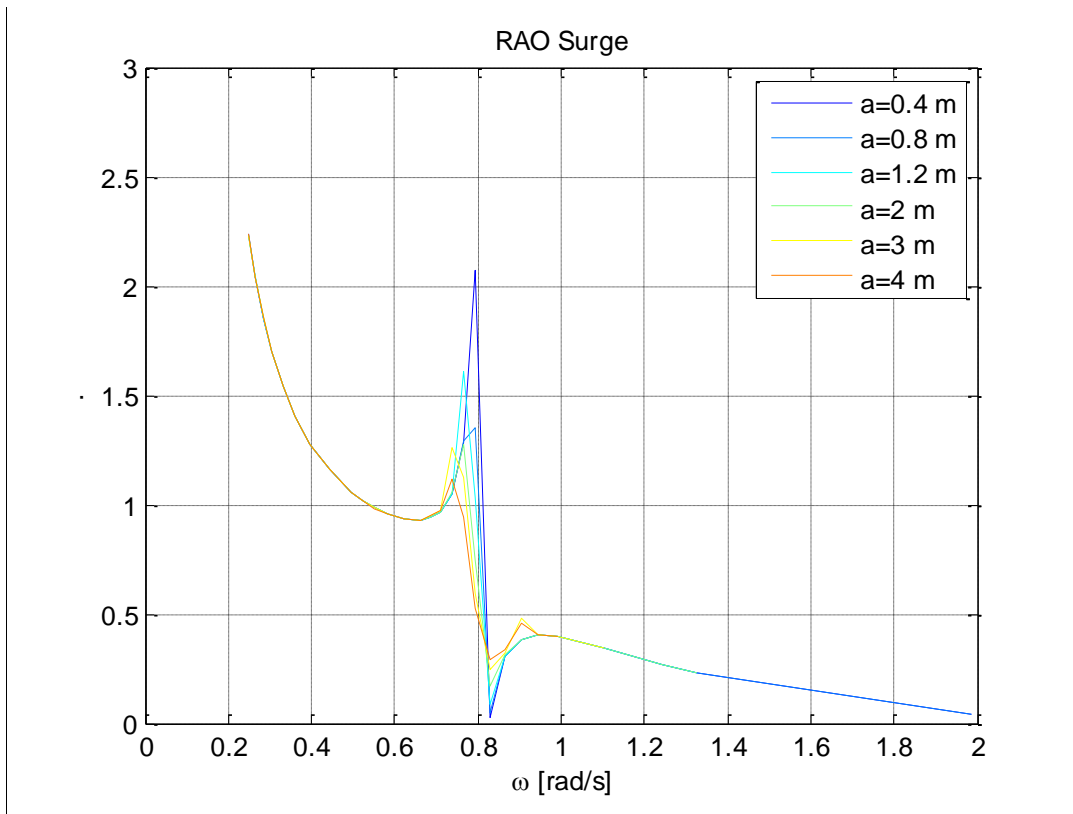


Figure 4-2 Response amplitude operator of buoy global surge

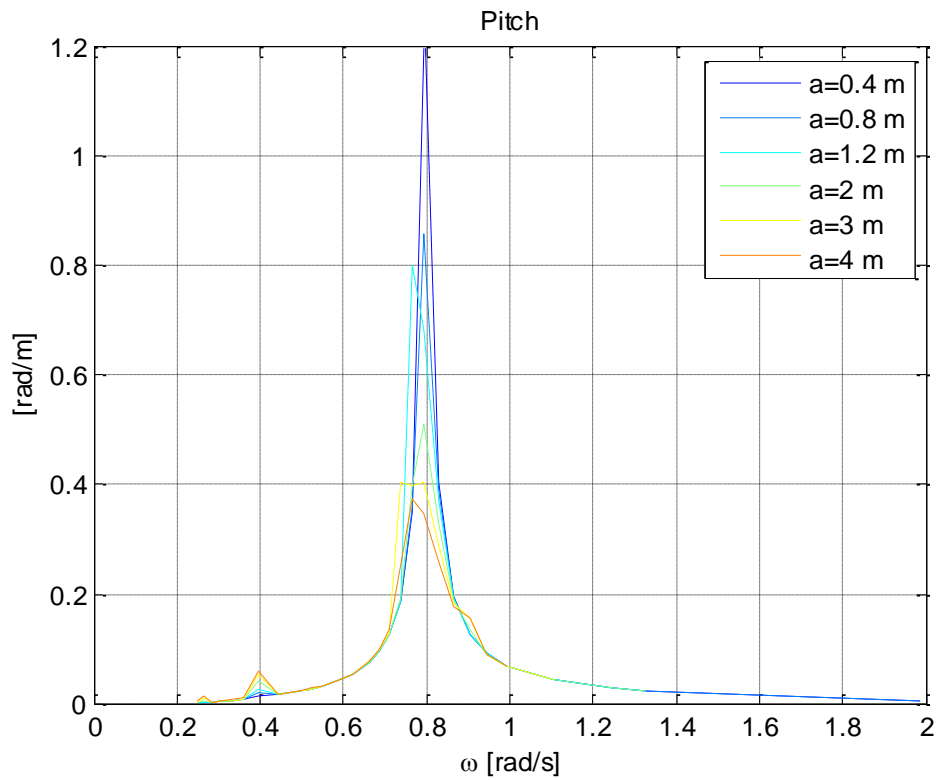


Figure 4-3 Response amplitude operator of buoy global pitch

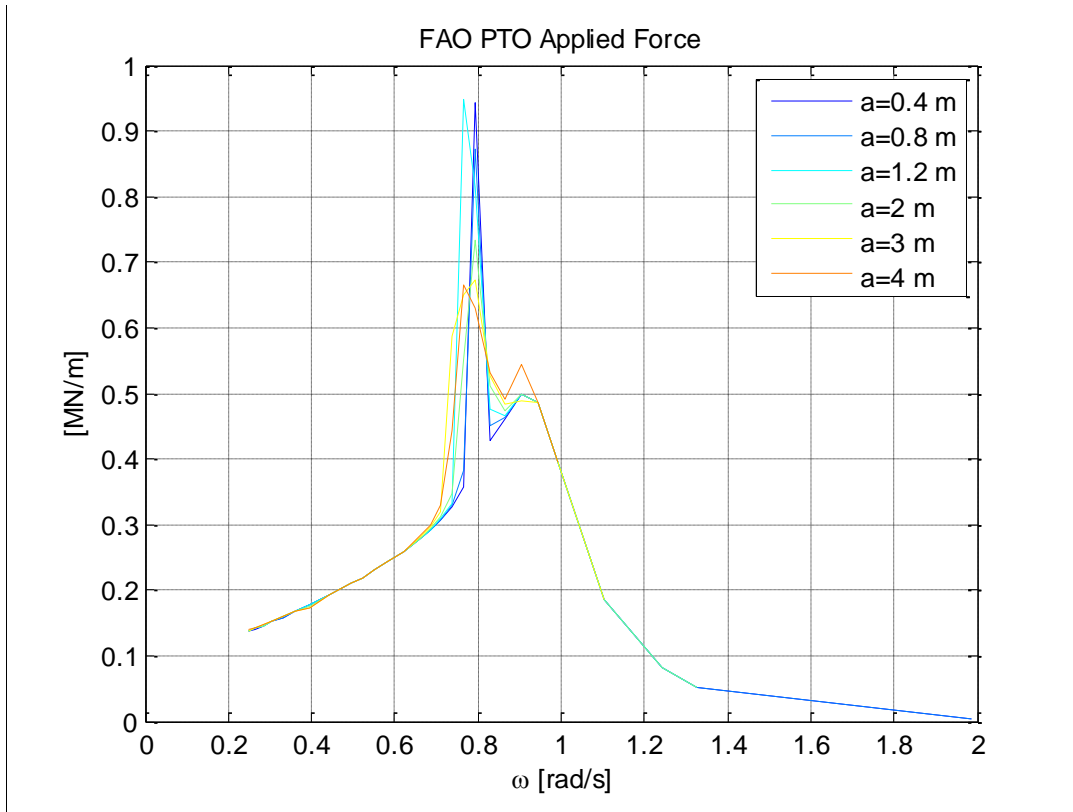


Figure 4-4 Force amplitude operator of PTO

The capture width is calculated using the 'Total System Power Take-Off (PTO) Performance' (PTO Power Output P) and dividing by the incident wave power per unit width P_w such that

$$l = \frac{P}{P_w} \quad (10)$$

Assuming deep water, the incident wave power is given by:

$$P_w = \frac{\rho\pi g^2 H^2 T}{8} \quad (11)$$

The relative capture width of the buoy is therefore given by $r = l/D$, where D is the diameter of the buoy. The relative capture width is shown in Figure 4-5. The two resonant motions due to pitching and heave result in larger power output at 0.8 and 0.9 rad/s. The most energy is extracted in the range of 0.6 to 1.2 rad/s (or wave period of 5 to 10 s) with the device extracting up to 3.5 times the incident wave power passing through its width (albeit for a very narrow band of frequencies). Note that the addition of viscous forces is likely to damp down the peaks of the relative capture width curves significantly.

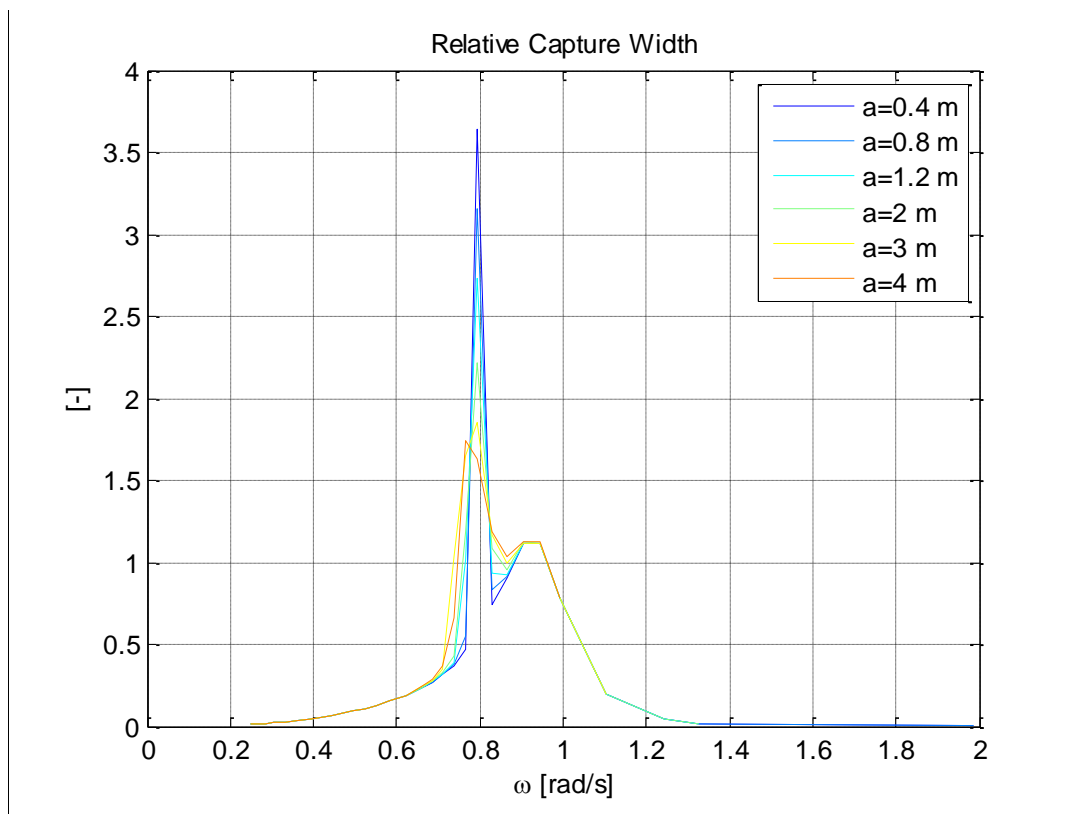



Figure 4-5 Relative capture width of point absorber

4.2 Unidirectional irregular sea states

Time domain simulations were conducted with irregular unidirectional waves as described in Section 2.1.1 (Case II). The minimum and maximum values throughout the time series are presented for the buoy kinematics, PTO forces and power output. The simulations have been run for 3 hours (equivalent full scale duration) in order to get reliable estimates of extreme values.

Prior to running simulations a calm water test was conducted to check the equilibrium position of the buoy on the still water surface. A calm water test is simulated by setting the height of all incoming waves to zero such that the buoy naturally reaches its equilibrium position during a time domain simulation. It was found that there is a mismatch between the initial position of the buoy at the beginning of the simulation and the rest location following the calm water test. This is due to a discrepancy between the buoyancy force of the buoy and the preload applied at the PTO spring which results in a 0.1 m extension of the spring in the heave direction at full-scale once the buoy has reached equilibrium. This offset will only affect the min/max outputs while the root mean square of time series outputs will be largely unaffected. A more comprehensive analysis, which could be considered in future, would involve re-running the flow solver using the new equilibrium position of the buoy (although it is anticipated that the resulting hydrodynamic coefficients will not change significantly).

The preload force was set in order to avoid snatch loads in the tether during simulations. For the verification data to be of most use, the results should be comparable to more high-fidelity computational fluid dynamic codes. It was decided that snatch loads, whilst potentially important, could mask the differences in hydrodynamic loading and so should be avoided in these investigations.



The maximum motions of buoy heave, pitch and surge for the are summarised in Figure 4-6, Figure 4-7 and Figure 4-8 respectively. The significant steepness S_e has been calculated for all sea states. The results are then curtailed by setting a limit for the steepness such that $S_e < 0.07$ must be satisfied. This removes all unrealistic sea states.

It can be seen that as the incident significant wave height increases, the buoy motions also increase. The maximum global heave excursion is relatively insensitive to energy period due to the range of periods contained within each sea state. The buoy pitch motion is generally greatest for energy periods around 8 s. This is in agreement with the shape of the RAO for pitch in Section 4.1.

The maximum values of the extension of the PTO joint and applied force acting on the joint are shown in Figure 4-9 and Figure 4-10 respectively. The applied force on the PTO is greatest when the wave height is large and the energy period is around 6 to 8 s such that the device is caused to resonate by the incident wave field. The PTO applied force in the numerical model is negative when the spring is in tension. The maximum values are never above zero (and as such, snatching loads do not occur). The maximum power output in Figure 4-11 shows a similar trend to the PTO applied force, with resonance causing larger power output close to an energy period of 6 to 8 s.

Minimum values of buoy motion for heave, pitch and surge are summarised in Figure 4-12, Figure 4-13 and Figure 4-14 respectively. The largest negative values of buoy heave excursion are directly related to significant wave height and the maximum negative pitching motions are observed around 8s. The minimum PTO spring displacement, PTO applied force and power absorption are presented in Figure 4-15, Figure 4-16 and Figure 4-17 respectively. The results show that the extreme displacements and forces acting on the device are approximately symmetric around the equilibrium position. In addition, the minimum power output of the device is 0 across all sea states as there are times when the spring velocity is 0 and therefore power is not generated.

As the wave conditions considered in this section are unidirectional, the results for buoy sway and roll motions have not been included. This type of motion is not expected for these wave conditions and analysis of the time series data found that the buoy roll and sway motions were negligible.

The root mean square (RMS) motions of the buoy are presented in Figure 4-18 and Figure 4-19 respectively. The range of heave motion is directly related to magnitude of oncoming waves while the range of pitching motion is largest when the oncoming waves have a wave period of roughly 8s.

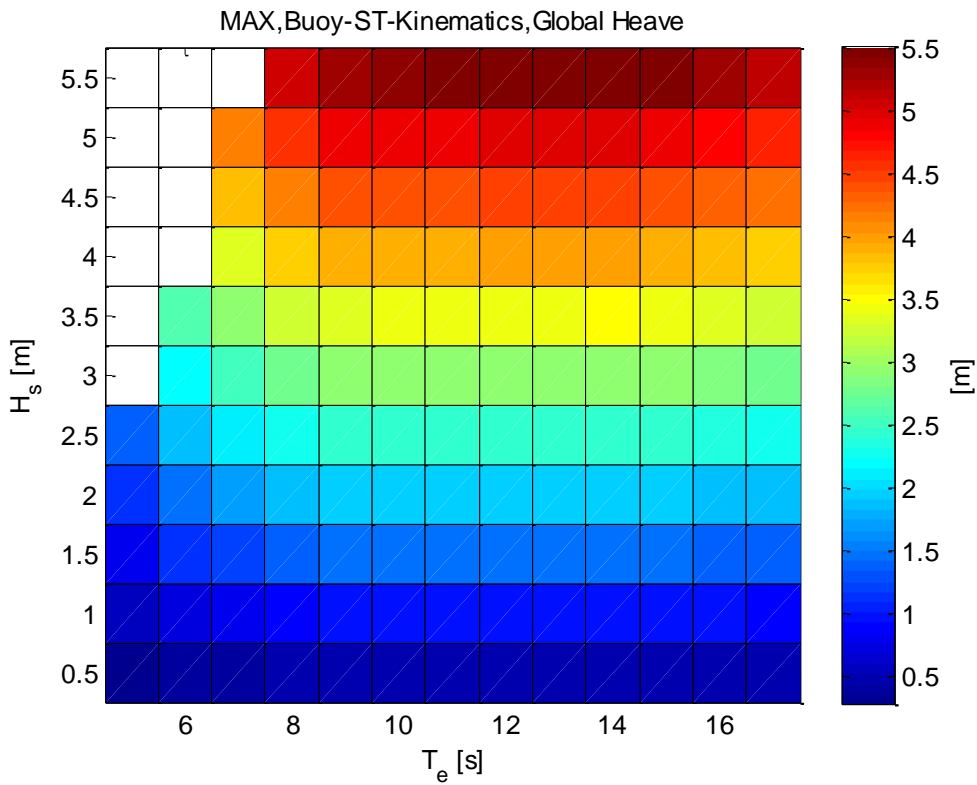


Figure 4-6 Max of global buoy heave for irregular unidirectional waves based on WETS scatter table

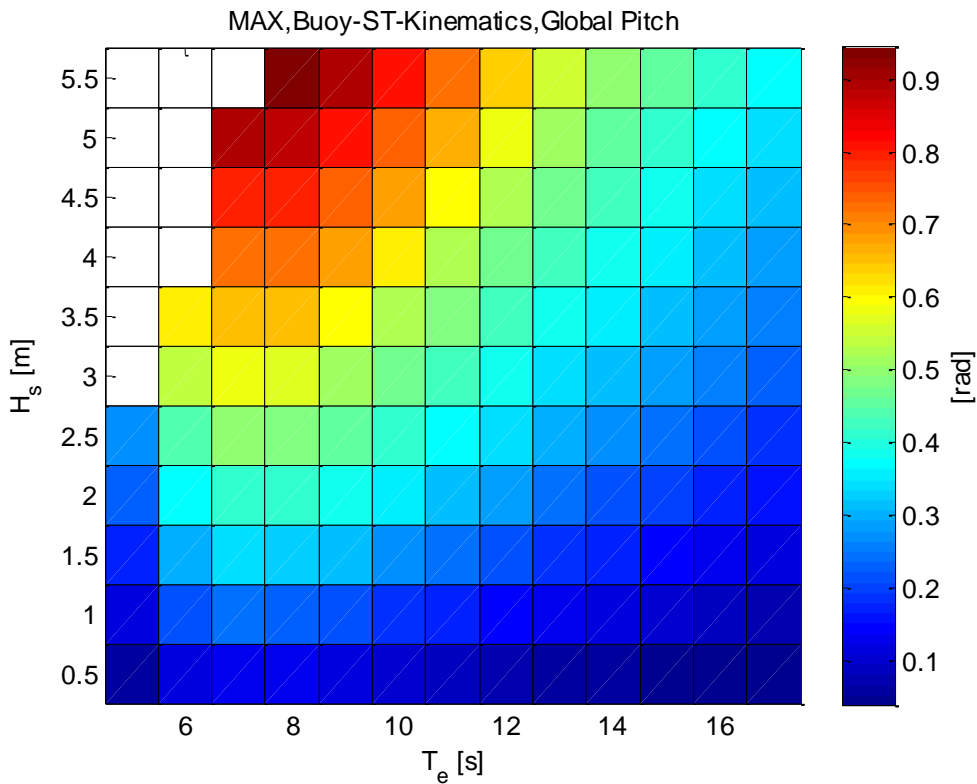


Figure 4-7 Max of global buoy pitch for irregular unidirectional waves based on WETS scatter table

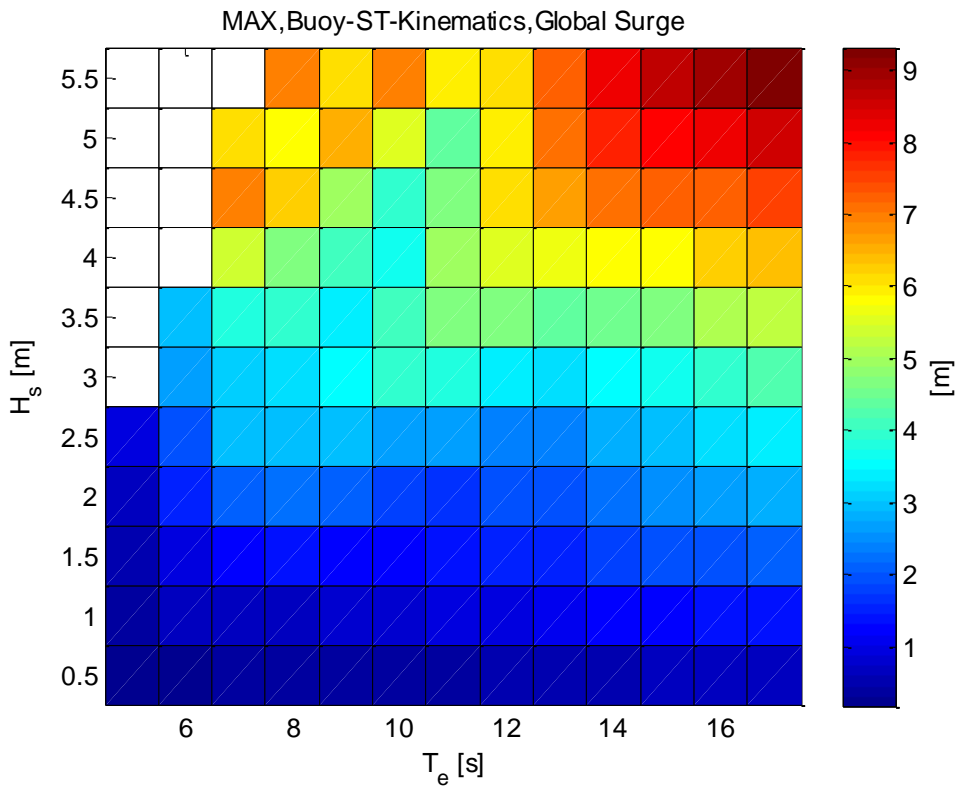


Figure 4-8 Max of global buoy surge for irregular unidirectional waves based on WETS scatter table

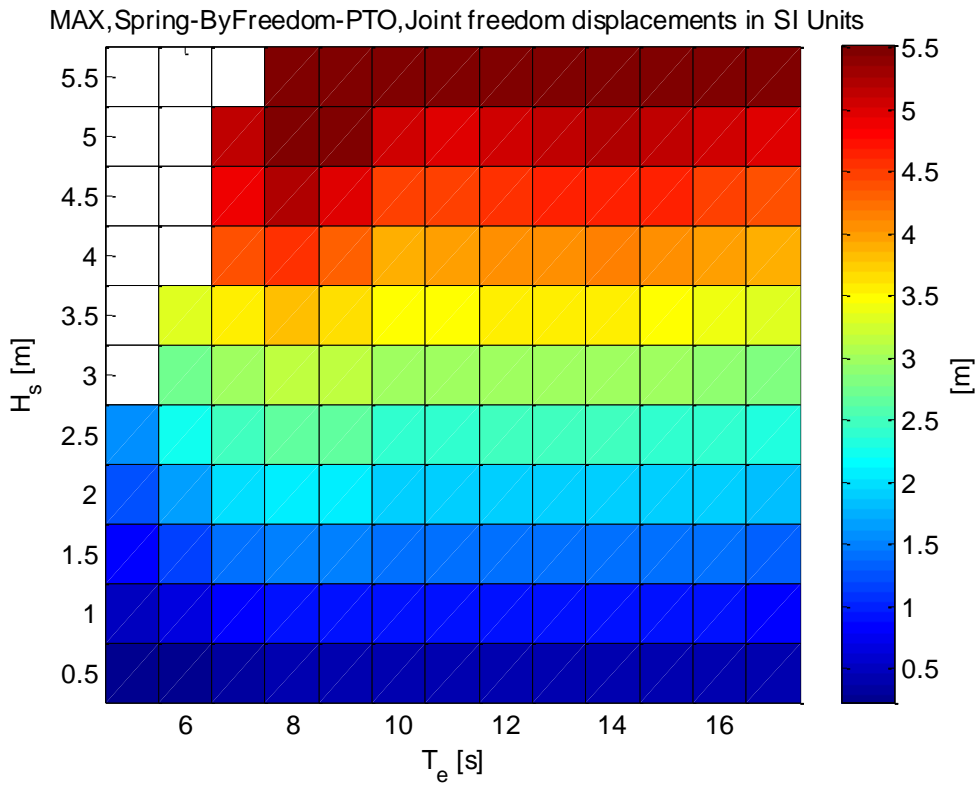


Figure 4-9 Max PTO joint freedom for irregular unidirectional waves based on WETS scatter table

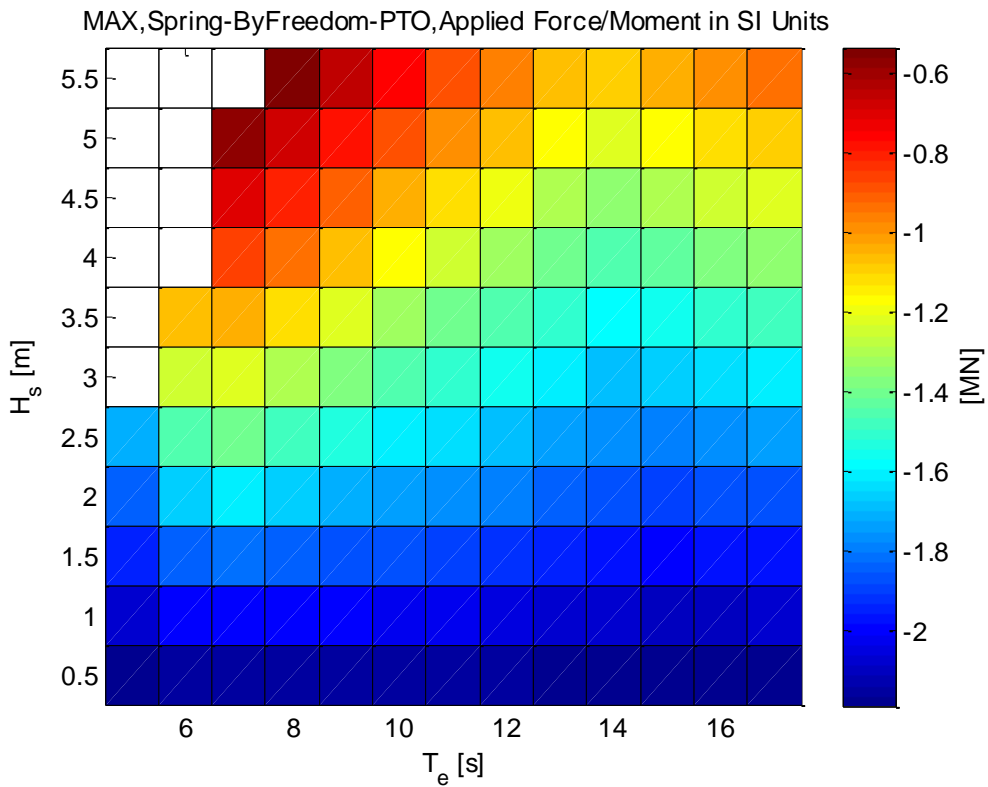


Figure 4-10 Max of PTO applied force for irregular unidirectional waves based on WETS scatter table

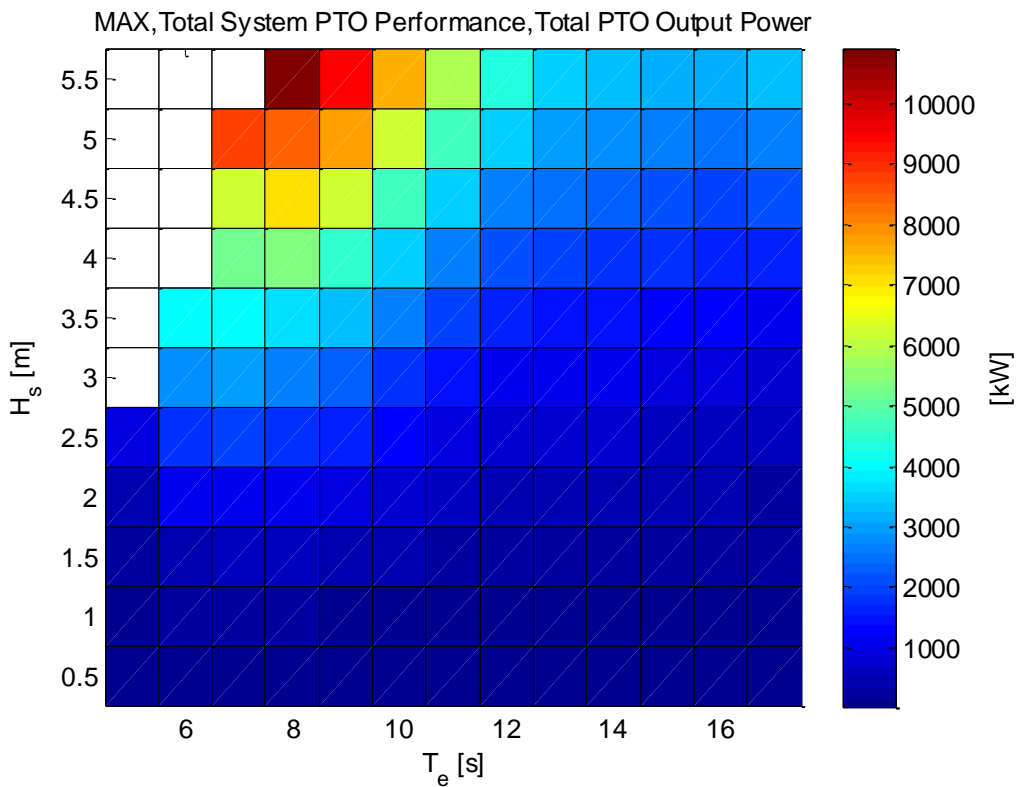


Figure 4-11 Max of PTO power output for irregular unidirectional waves based on WETS scatter table

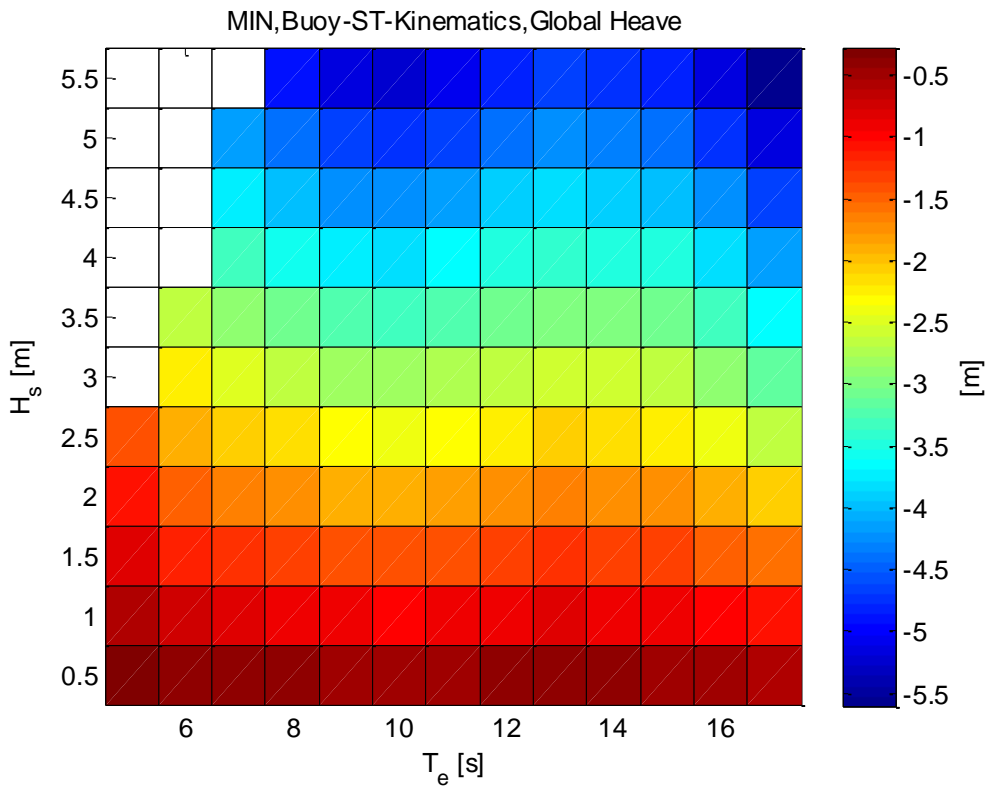


Figure 4-12 Min global heave for irregular unidirectional waves based on WETS scatter table

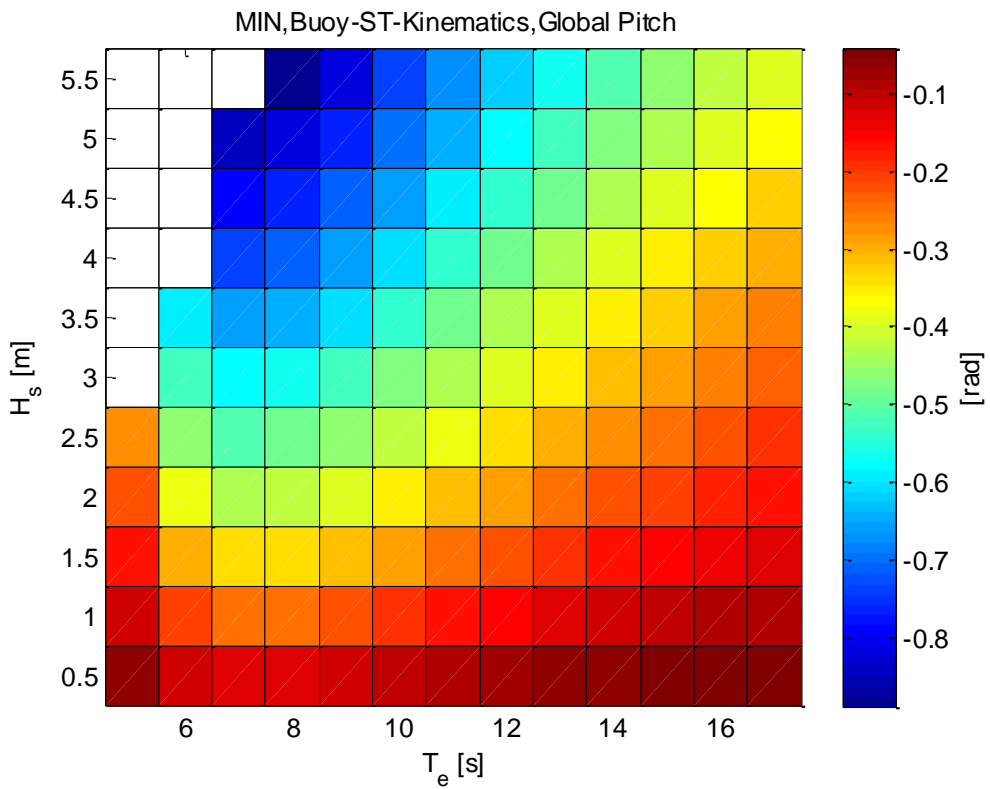


Figure 4-13 Min global pitch for irregular unidirectional waves based on WETS scatter table

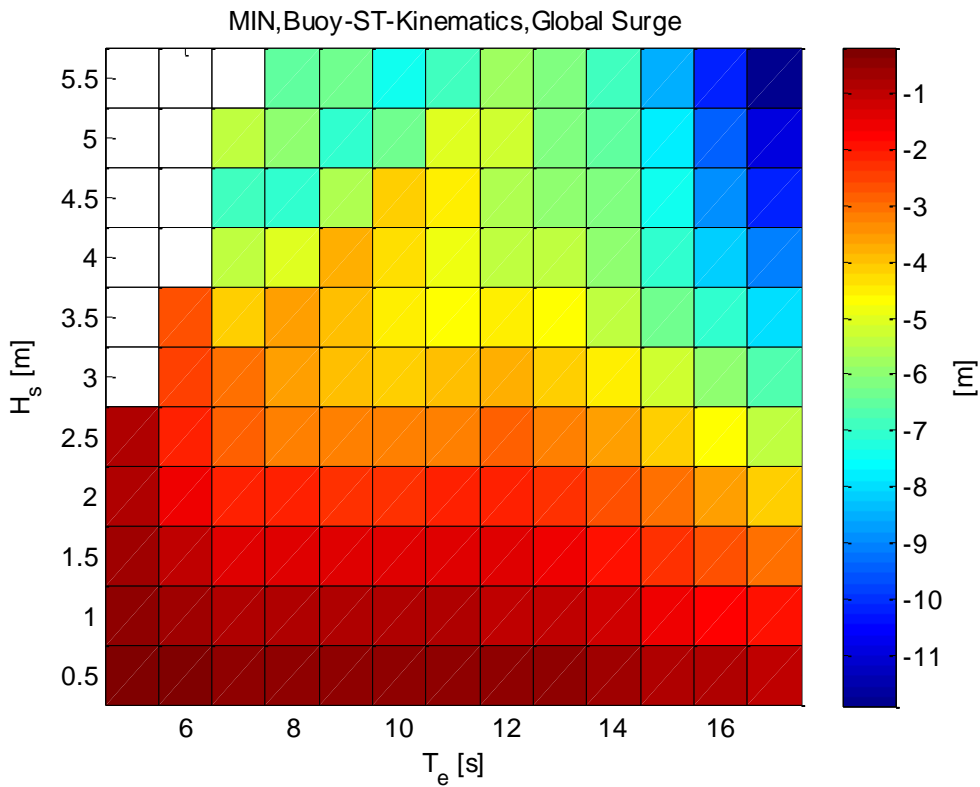


Figure 4-14 Min global surge for irregular unidirectional waves based on WETS scatter table

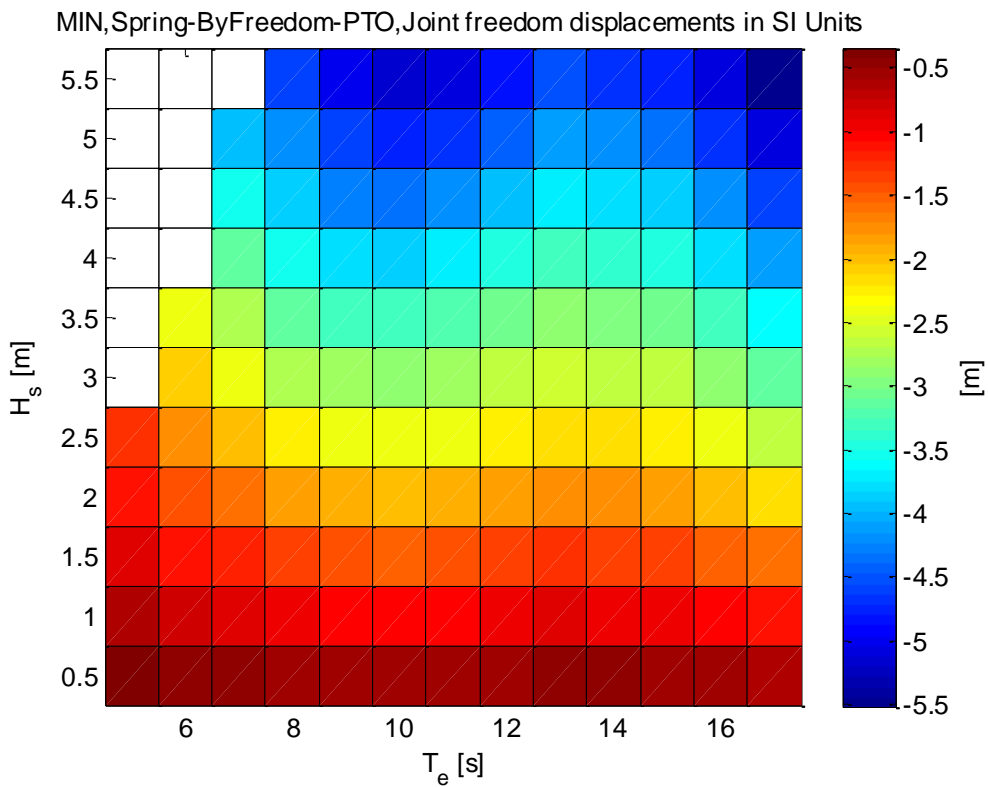


Figure 4-15 Min global PTO spring freedom for irregular unidirectional waves based on WETS scatter table

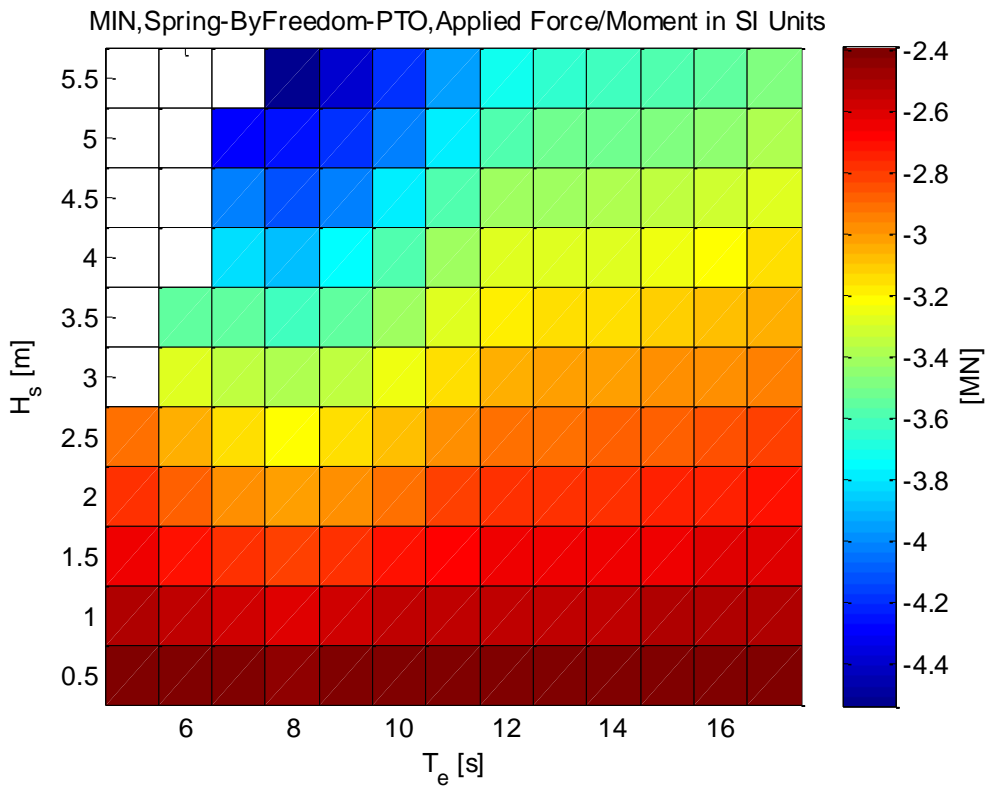


Figure 4-16 Min PTO applied force for irregular unidirectional waves based on WETS scatter table

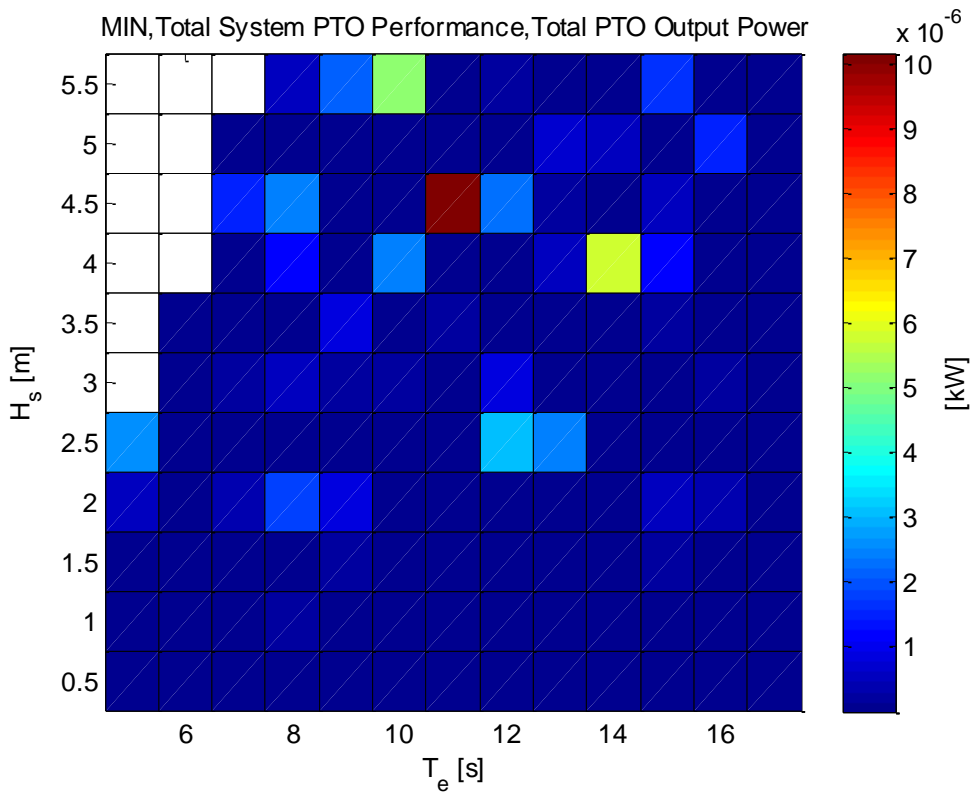


Figure 4-17 Min of PTO power output for irregular unidirectional waves based on WETS scatter table

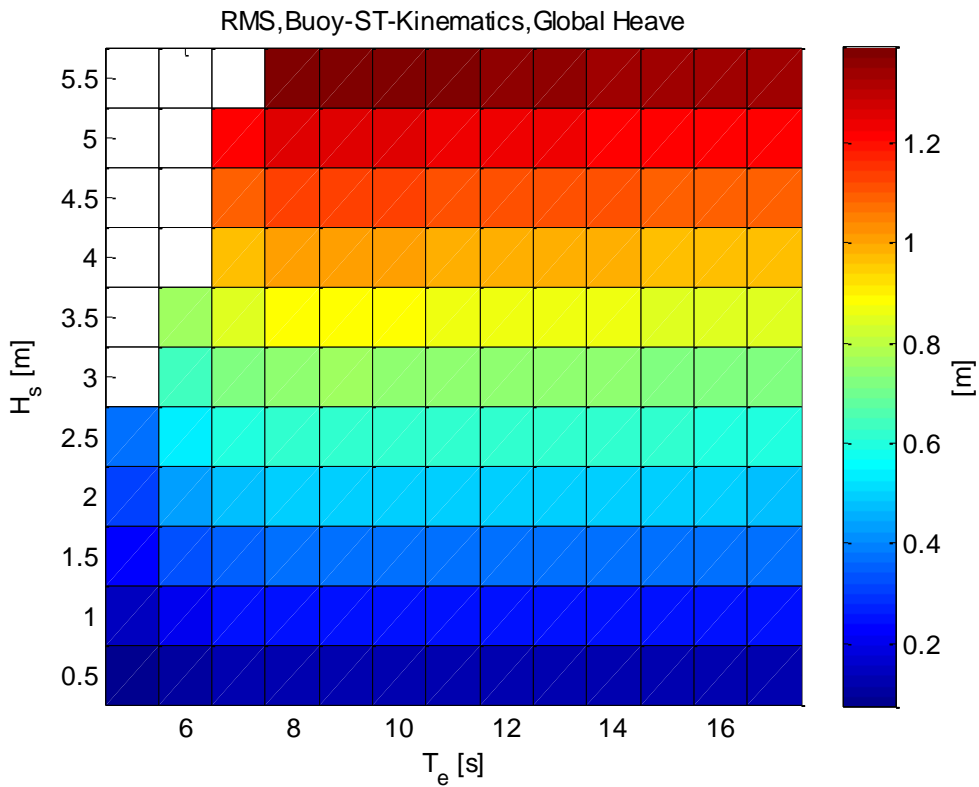


Figure 4-18 RMS of buoy heave for irregular unidirectional waves based on WETS scatter table

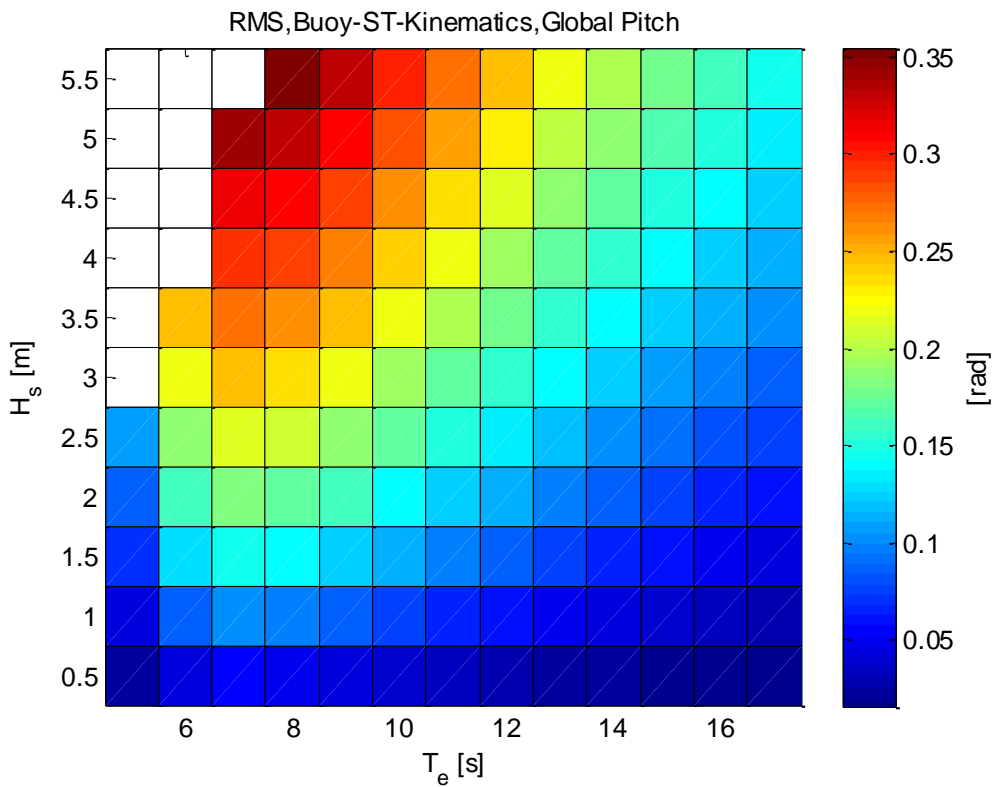


Figure 4-19 RMS of buoy pitch for irregular unidirectional waves based on WETS scatter table

4.3 Irregular spread waves

Time domain simulations were conducted with irregular spread waves as described in Section 2.1.1 (Case III). The simulations have been run for 30 minutes (full-scale equivalent duration). The RMS values of the time series results are presented for the buoy kinematics, PTO forces and power output. As before the results must satisfy $S_e < 0.07$ such that all unrealistic sea states are removed.

The RMS of buoy heave and pitch motions are presented in Figure 4-20 and Figure 4-21 respectively. The results of heave are similar to those in Section 4.2 with a similar range of motions observed. The RMS of pitch motions in the spread waves scenario are slightly different from the unidirectional case presented in Figure 4-19.

The addition of a degree of freedom in the hinges (see Section 3) enables roll and global sway motions of the buoy to be captured. The sway, surge and roll motions are presented in Figure 4-22, Figure 4-23 and Figure 4-24. The range of roll motion is reasonable with the largest RMS values being around 20 degrees. The RMS sway motions are also large with up to 4 m of motion for a sea state of $H_s=5.5$ m and $T_e=10$ s. Both the sway and roll motions appear to have a resonance at a similar frequency to the pitching motions (which is due to the axi-symmetry of the WEC) as the largest motions are observed close to an energy period 8-10 s. The time series of the buoy global sway motions was investigated. A simulation for a sea state where the energy period was close to the pitch and surge resonant frequency and another simulation away from the resonant frequency were compared in Figure 4-25. It can be seen that with time the buoy sway motions grow. This is thought to be due to resonance in the mooring. It is possible that in reality viscous effects which are not modelled in the simulations would damp this motion.

The RMS of the PTO joint displacement and applied force are provided in Figure 4-26 and Figure 4-27 respectively. The buoy natural resonances can be observed in the PTO joint displacement which shows a large range at roughly an 8-10 s energy period. The RMS of PTO applied force is sensitive to both wave period and wave height.

The RMS and Mean of total PTO power output is presented in Figure 4-28 and Figure 4-29. The total PTO power output is defined as the power absorbed by the damper before any losses in the electrical system are taken into account. It can be seen that the largest power output occurs at $\omega \approx 0.9$ which matches the resonant frequency of the device.

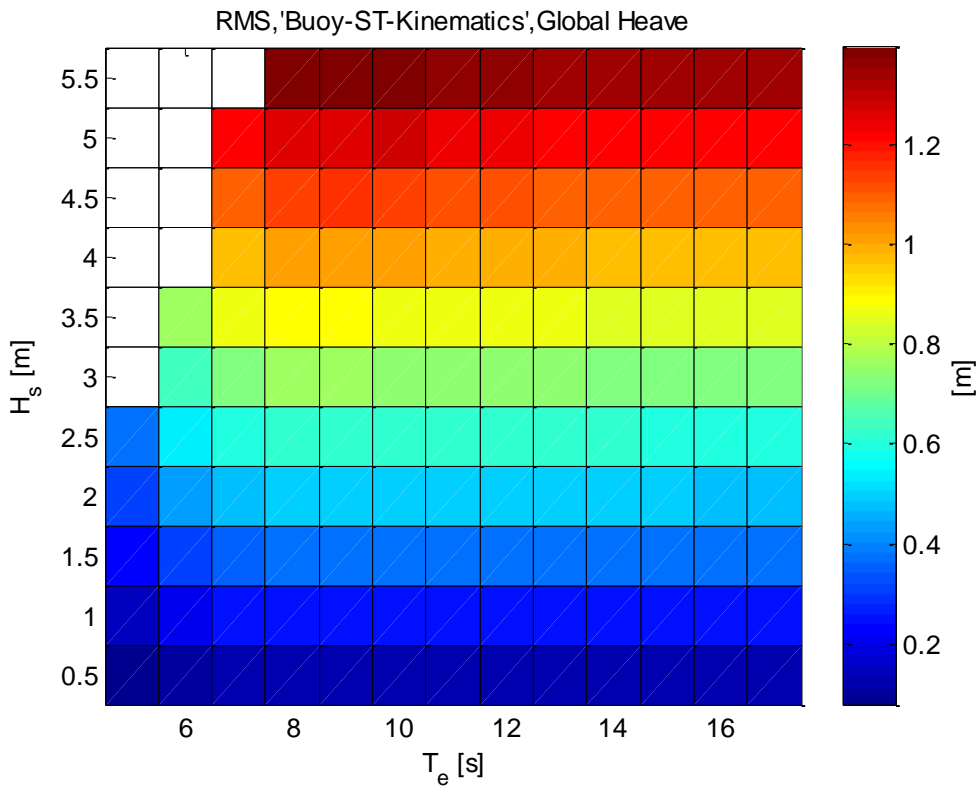


Figure 4-20 RMS of global buoy heave for irregular spread wave conditions and WETS scatter table

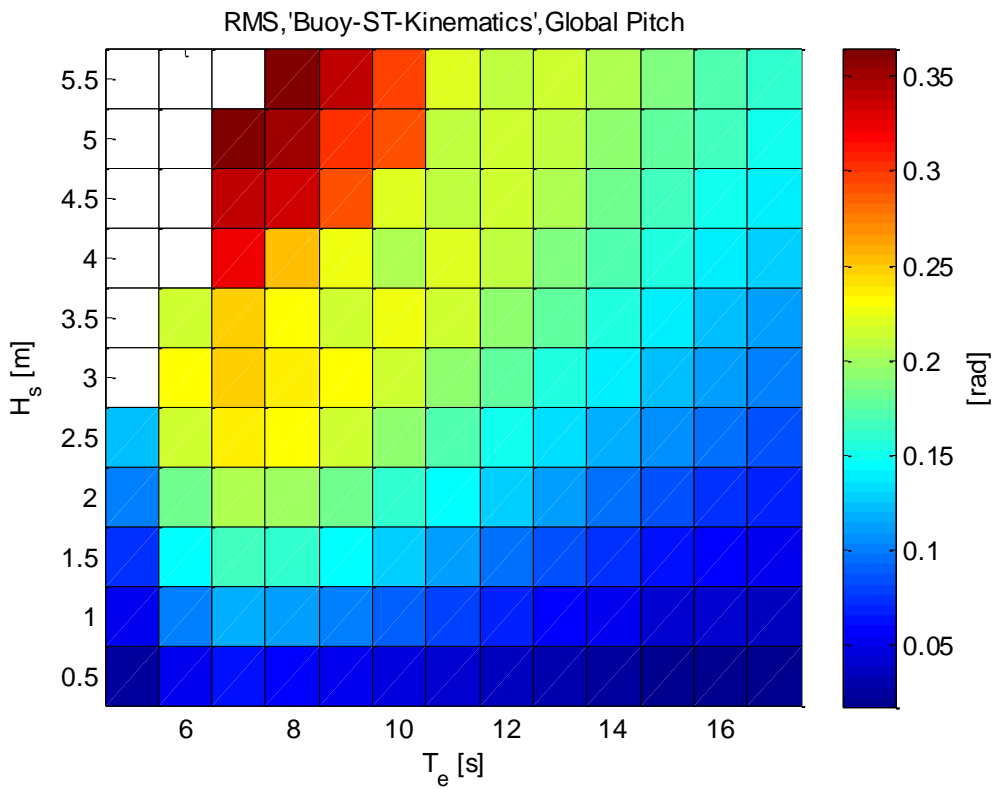


Figure 4-21 RMS of global buoy pitch for irregular spread wave conditions and WETS scatter table

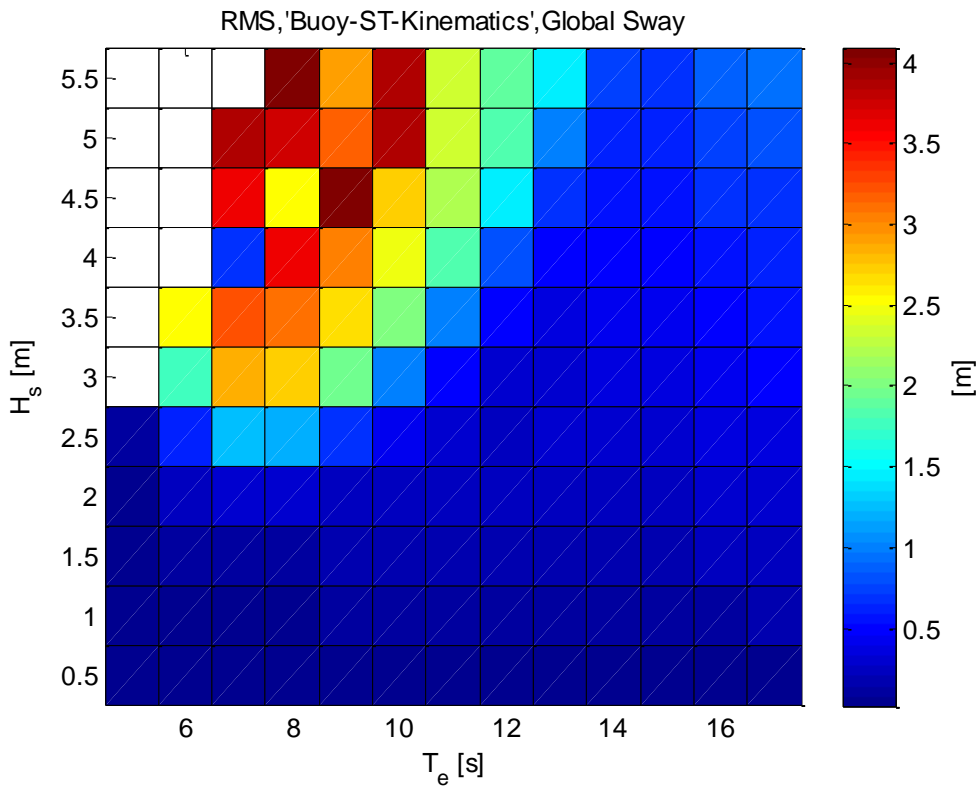


Figure 4-22 RMS of global buoy sway for irregular spread wave conditions and WETS scatter table

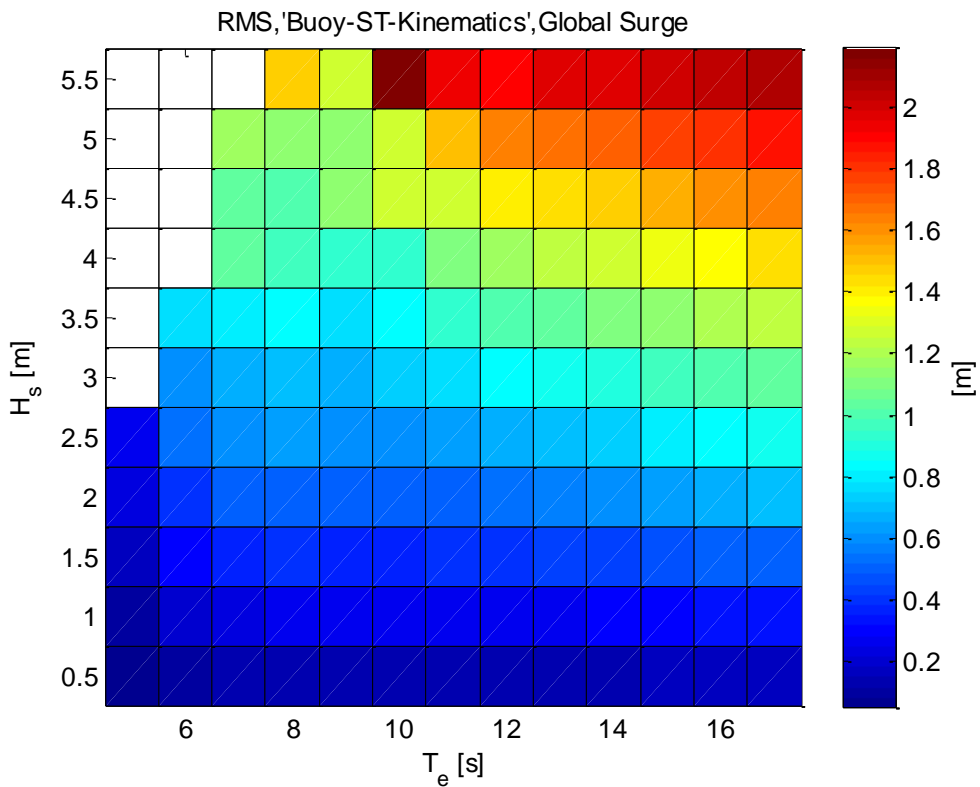


Figure 4-23 RMS of global buoy surge for irregular spread wave conditions and WETS scatter table

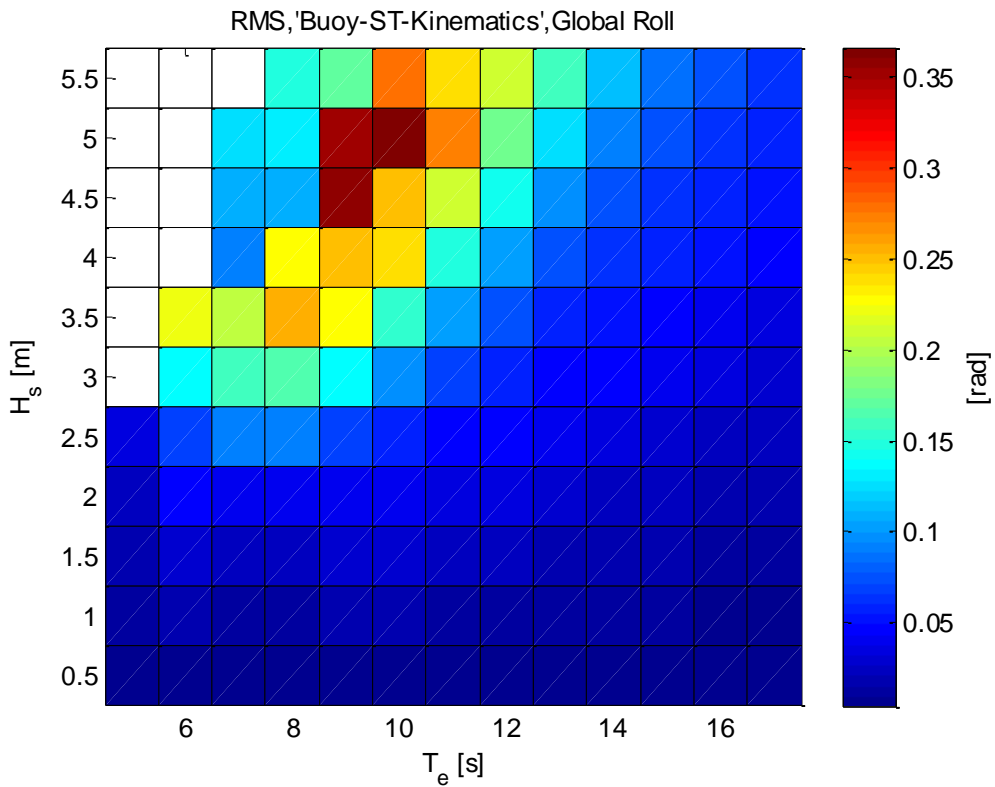


Figure 4-24 RMS of global buoy roll for irregular spread wave conditions and WETS scatter table

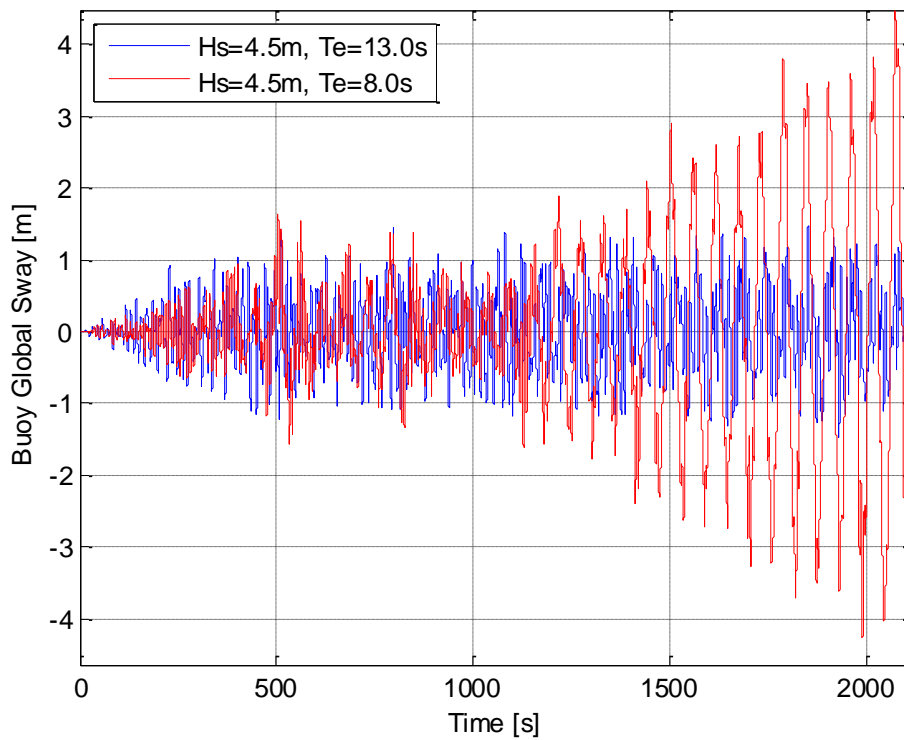


Figure 4-25 Time series comparison of ϕ_y for two sea states where mooring lines does and does not occur.

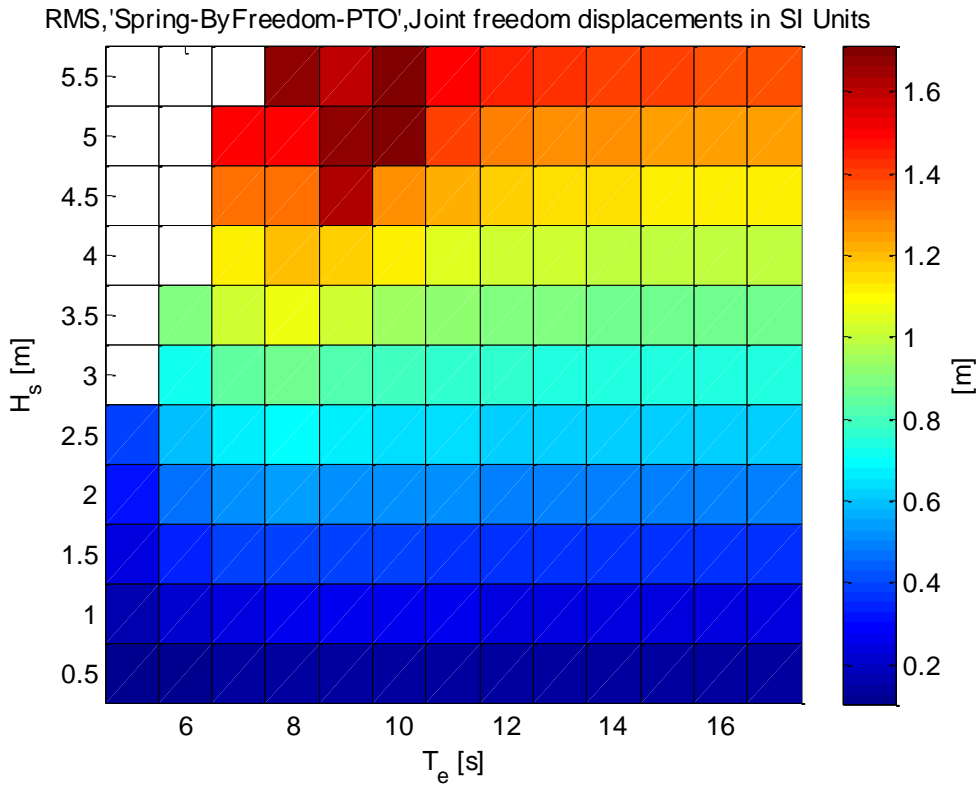


Figure 4-26 RMS of PTO joint displacement for irregular spread wave conditions and WETS scatter table

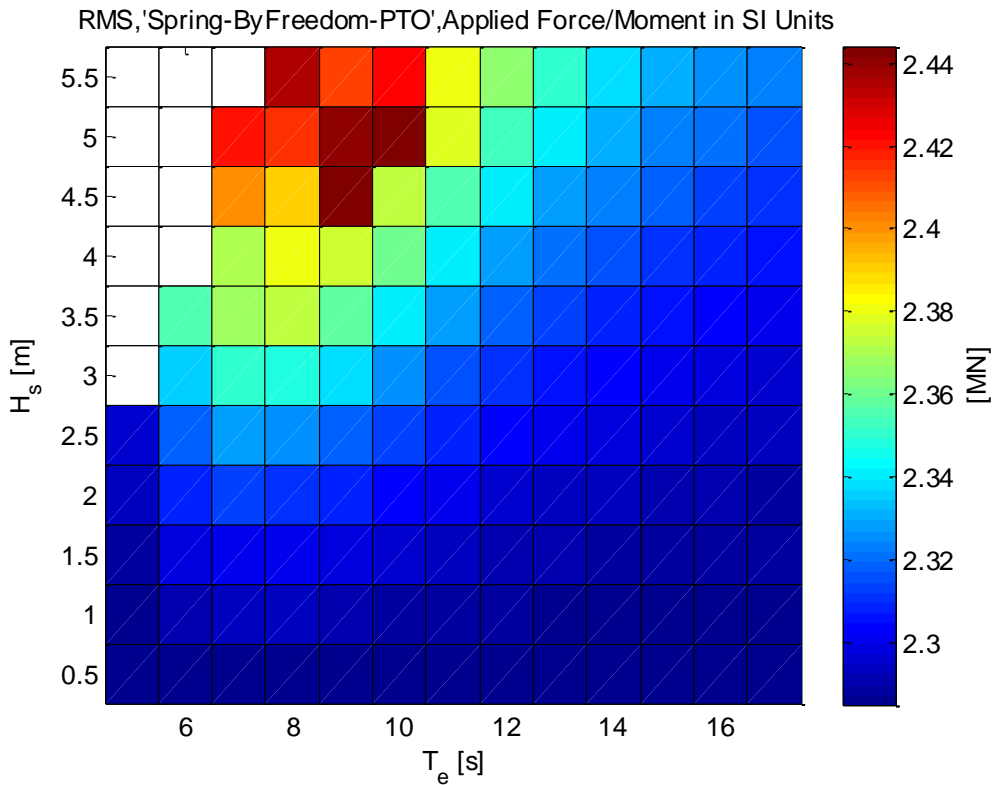


Figure 4-27 RMS of PTO applied force for irregular spread wave conditions and WETS scatter table

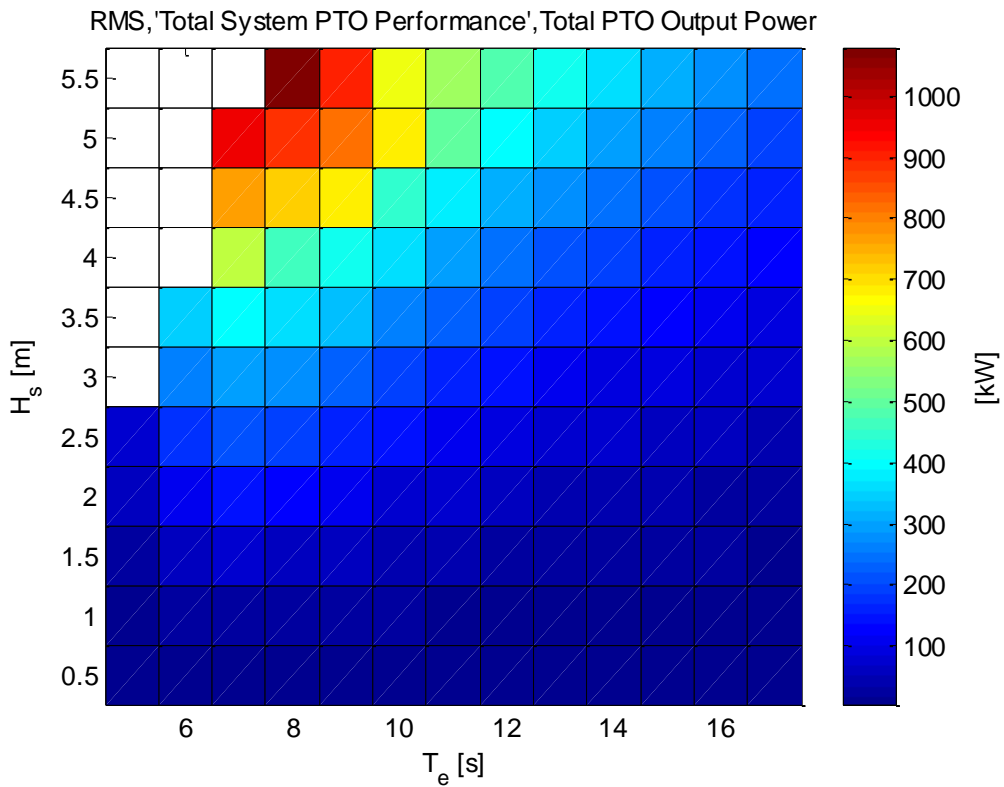


Figure 4-28 RMS of power output for irregular spread wave conditions and WETS scatter table

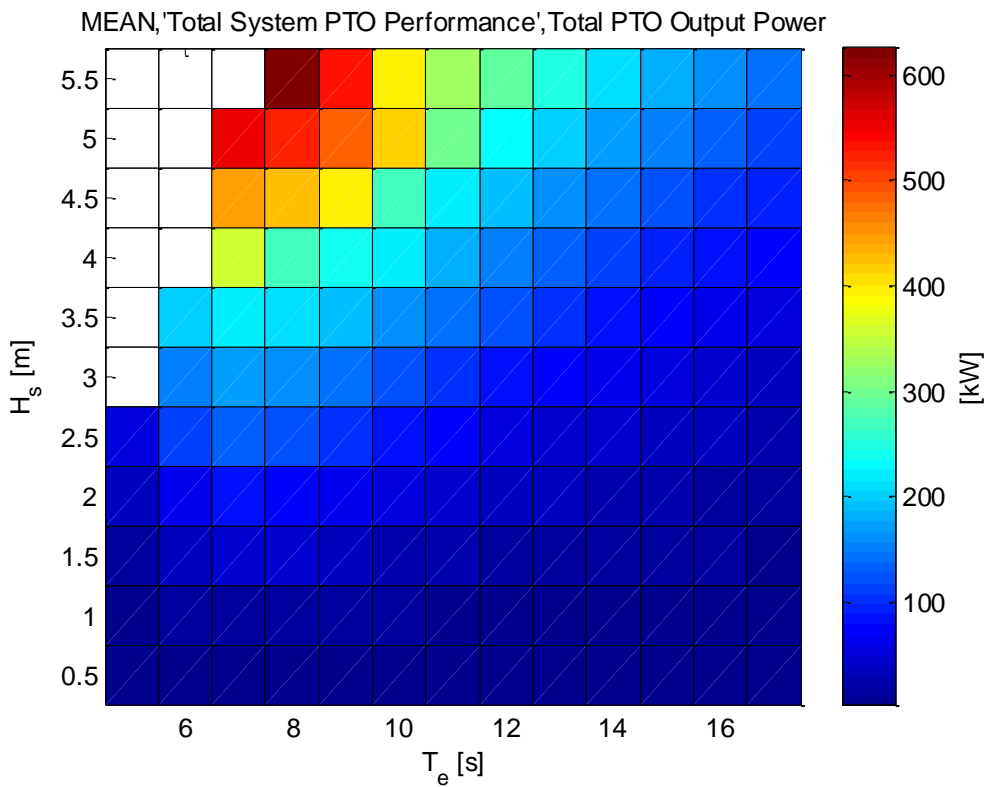


Figure 4-29 MEAN PTO power output for irregular spread wave conditions and WETS scatter table



4.4 Extreme response analysis

This section considers the device response to extreme wave conditions. Time domain simulations were conducted using the wave conditions described in Case IV.

However, an incident irregular wave field which describes normal operational conditions could still yield a larger force on the PTO than an extreme sea state due to the potentially complex dependence of load on incident wave elevation and motion time history. The ultimate limit state derived from normal operational wave conditions is investigated in Section 4.4.1. This is then compared to the ULS from the simulation of an extreme sea state in 4.4.2.

4.4.1 Normal operational sea states

Time series data from numerical simulations conducted using the normal operational conditions described for case II were analysed to identify the sea state for which the maximum PTO load occurs. In the numerical model, the PTO force is negative and therefore the maximum absolute value of the PTO force is used to identify the largest PTO loads. A 50 second sample was extracted around the point at which the maximum PTO load occurs. Figure 4-30 shows the time series output for the identified simulation.

The maximum PTO load does not coincide with maximum heave. Instead it coincides with peak pitch and surge motion instead. This is consistent with the findings of the response amplitude operators in Section 4.1 which showed that the machine is highly responsive to pitch motions at and around the frequency 0.8 rad/s.

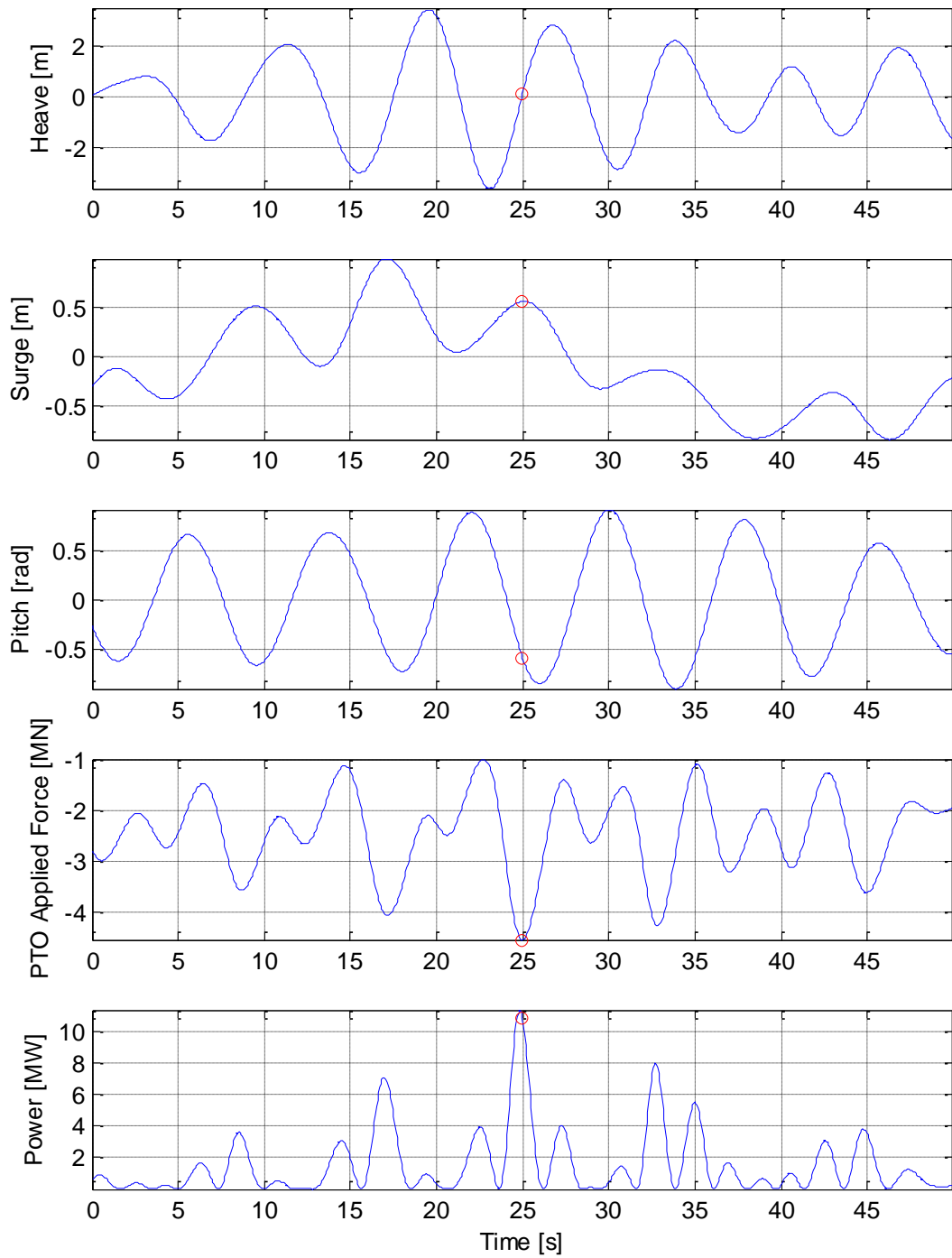


Figure 4-30 Time series of buoy position, load and power output around peak PTO applied force during normal wave conditions (case II) $H_s=5.5$ m and $T_e=7$ s.



4.4.2 Extreme sea states

A similar analysis was repeated for the time domain simulations. This time, the sea state where the maximum PTO load occurred when simulating extreme sea states (case IV) was identified. The time series data is presented in Figure 4-31. Again the peak load coincides with peak surge and pitch rather than heave.

Matrices of the global buoy heave, pitch, PTO forces and power output are presented in Figure 4-32 to Figure 4-39. The results are similar to those presented in Section 4.2. The buoy heave motion responds primarily to wave height while buoy pitch is sensitive to wave period. The PTO loads and power output are sensitive to both the buoy resonances and the wave height.

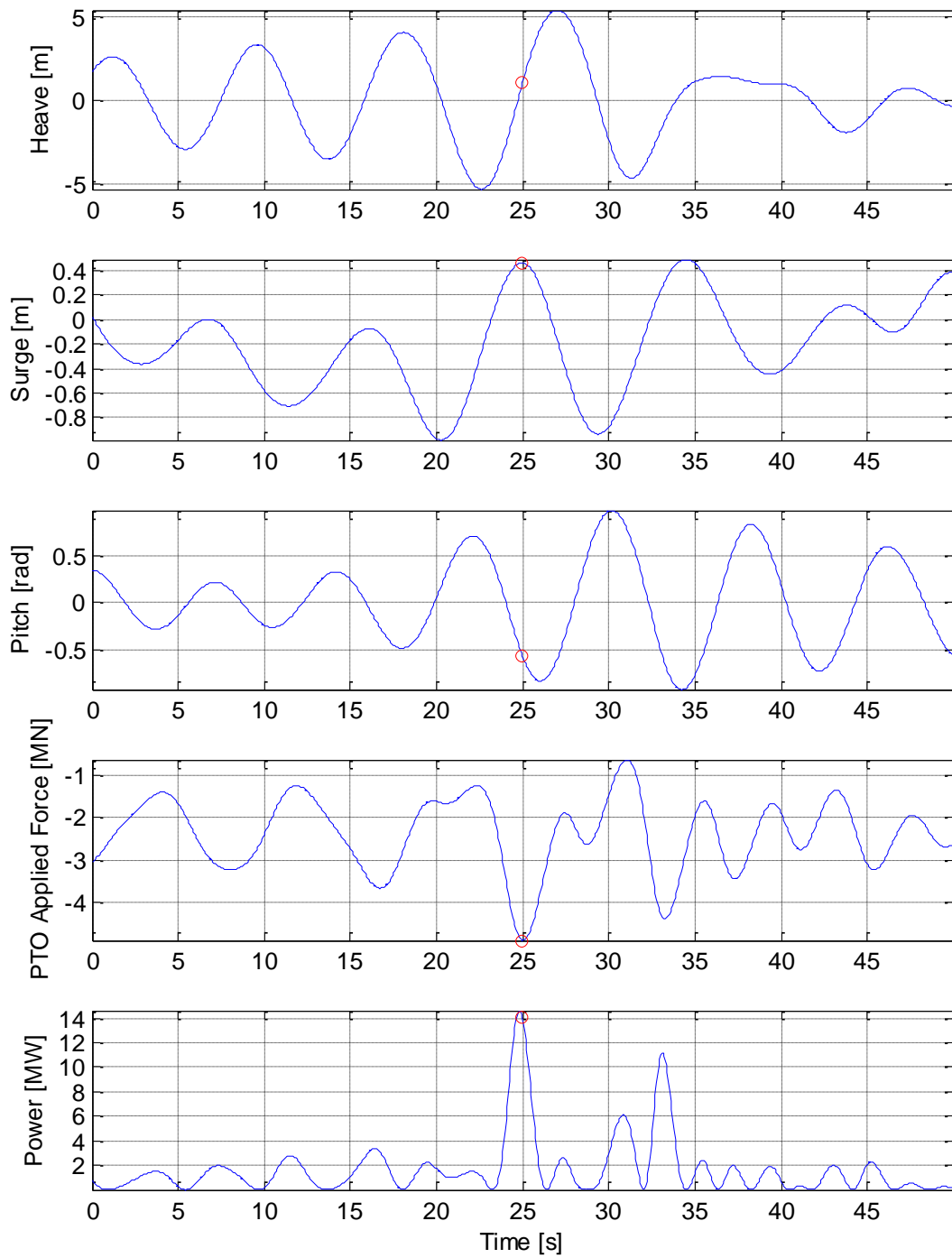


Figure 4-31 Time series of buoy position, load and power output around peak PTO applied force for extreme wave conditions (case IV) $H_s=6.87$ m and $T_e=9.6$ s.

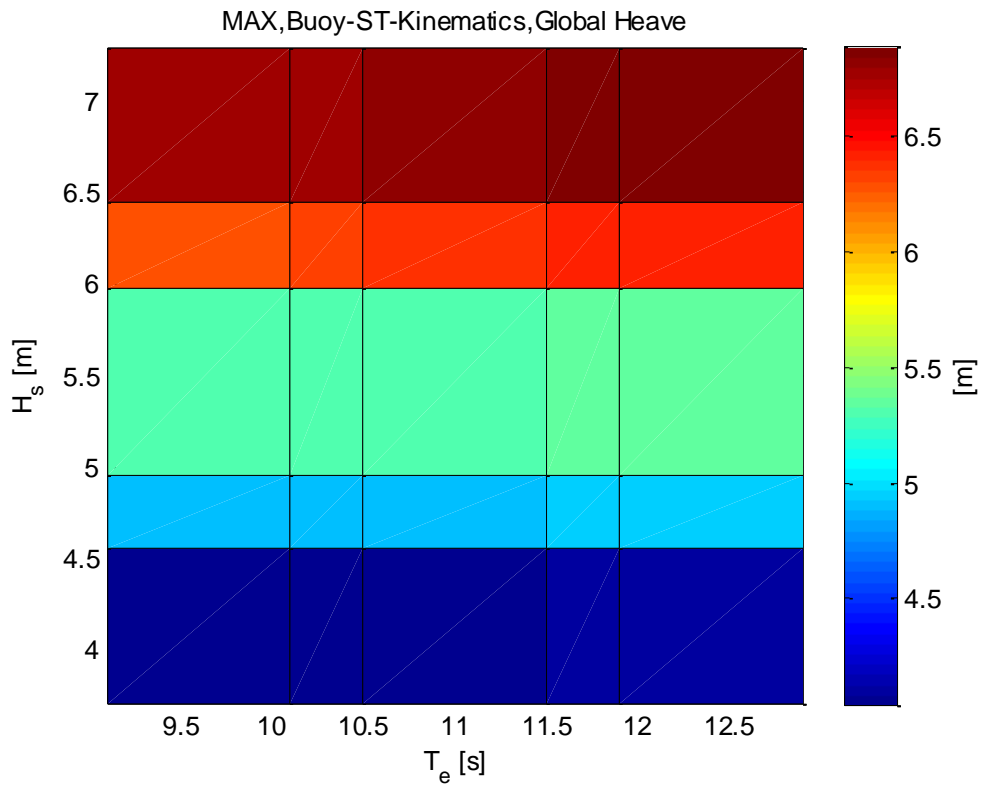


Figure 4-32 Max of global buoy heave for irregular unidirectional extreme waves

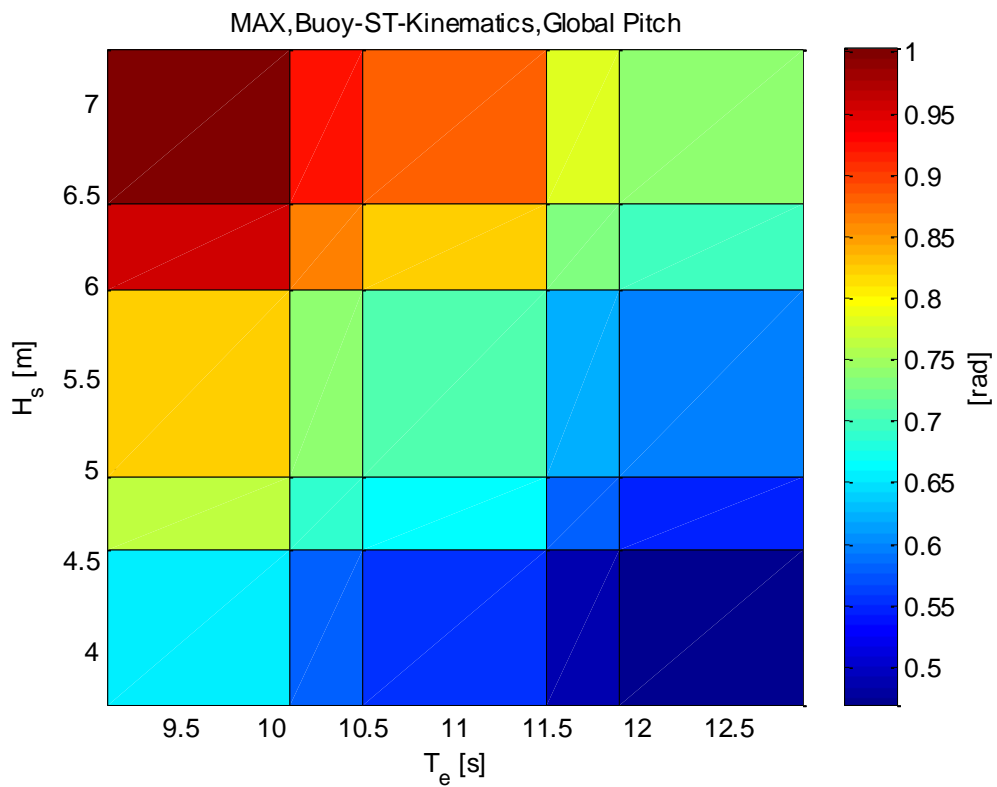


Figure 4-33 Max of global buoy pitch for irregular unidirectional extreme waves

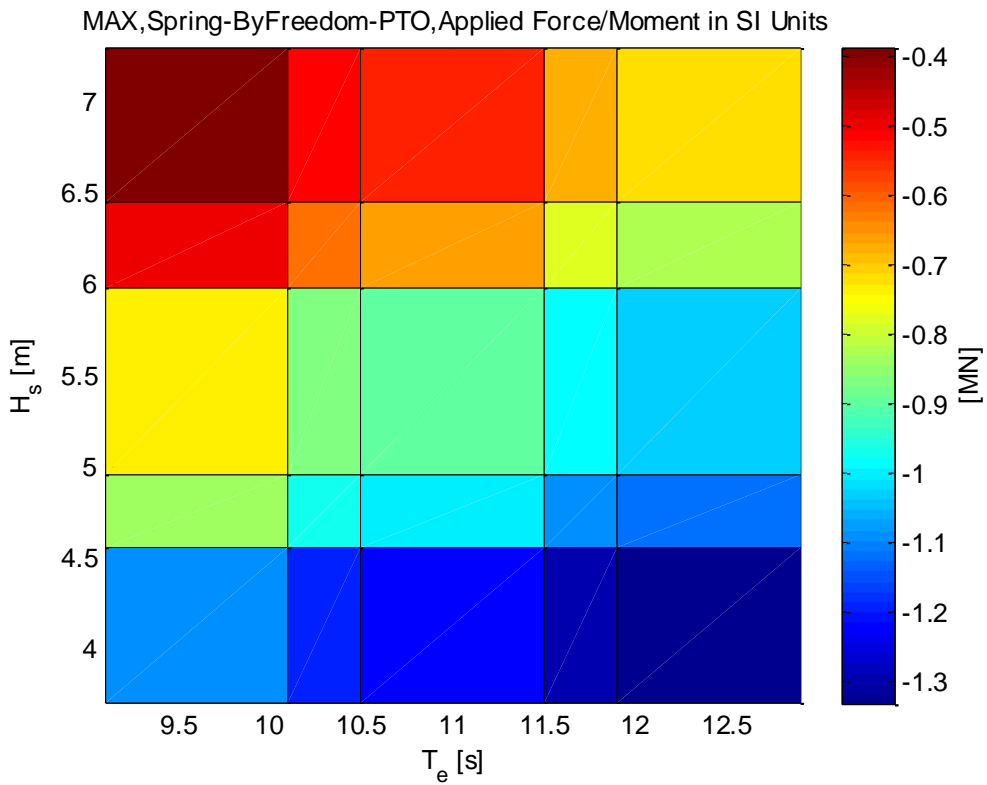


Figure 4-34 Max of PTO applied force for irregular unidirectional extreme waves

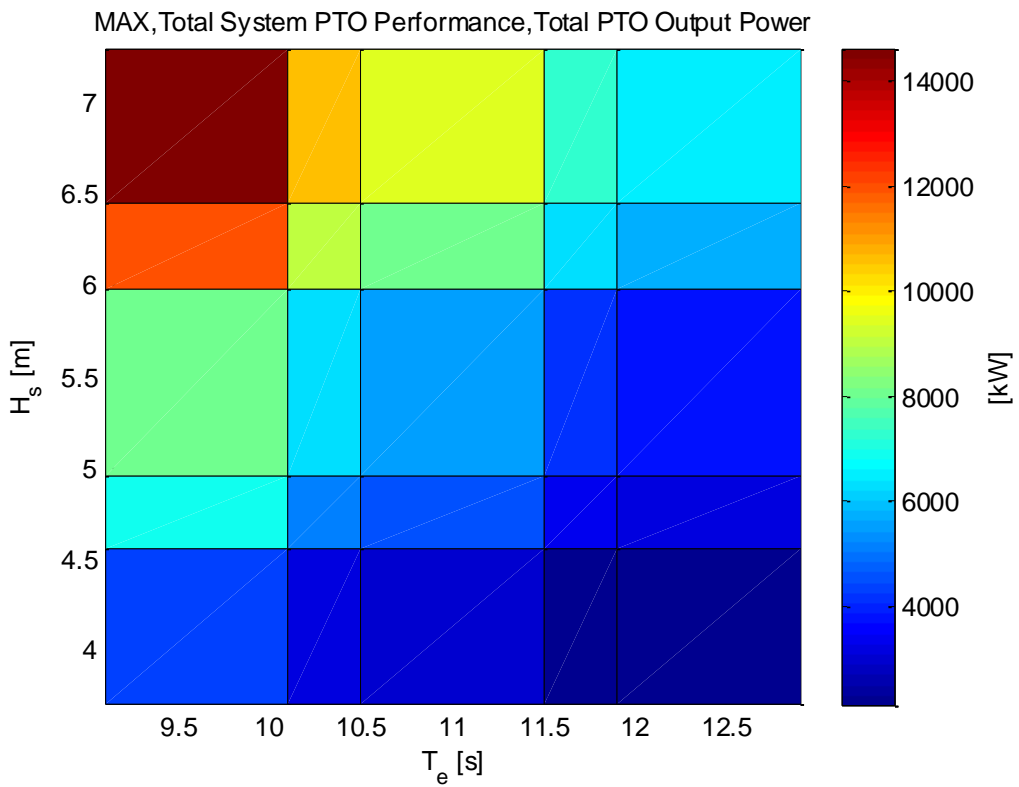


Figure 4-35 Max of PTO power output heave for irregular unidirectional extreme waves

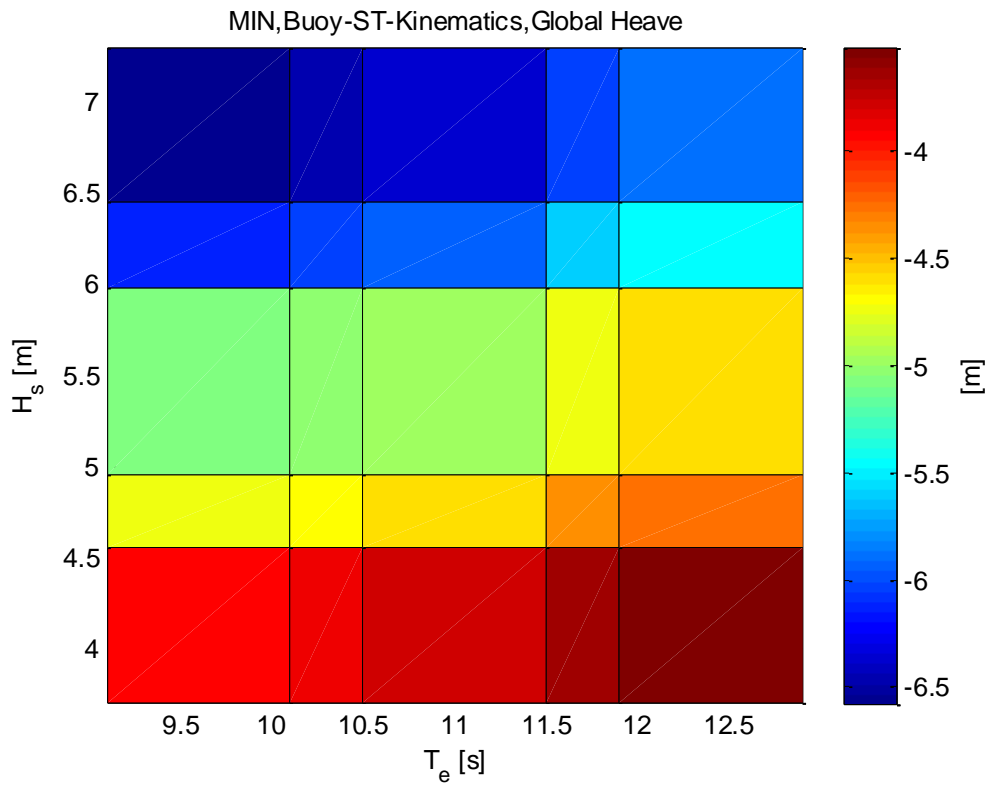


Figure 4-36 Min of global buoy heave for irregular unidirectional extreme waves

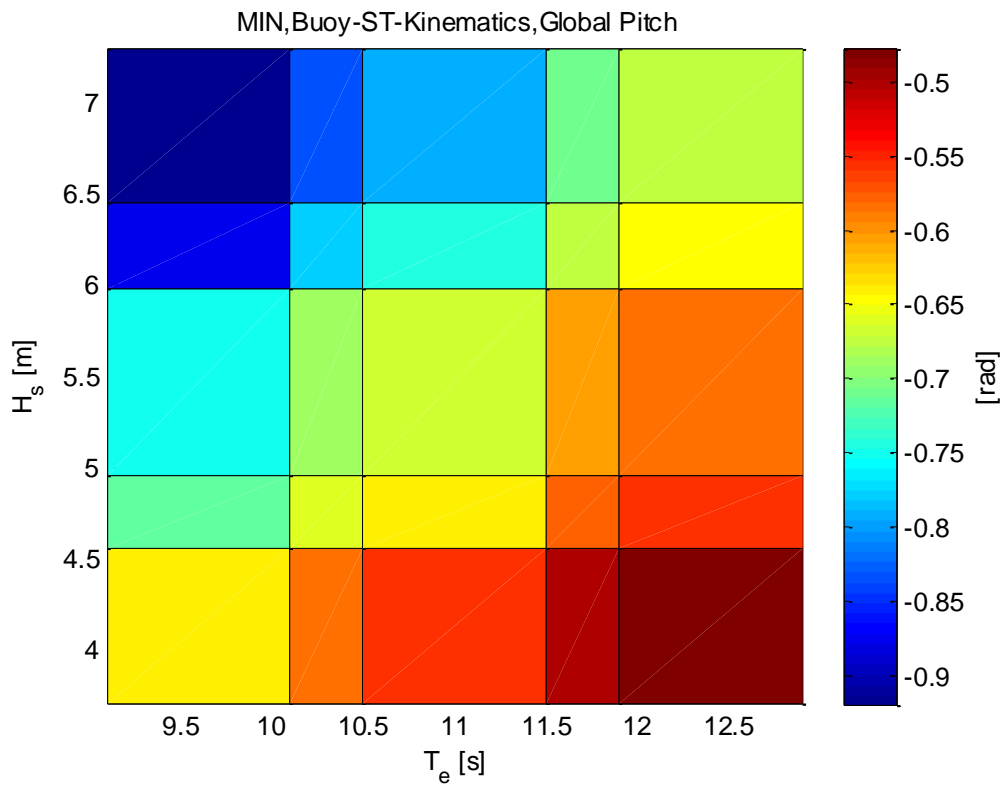


Figure 4-37 Min of global buoy pitch for irregular unidirectional extreme waves

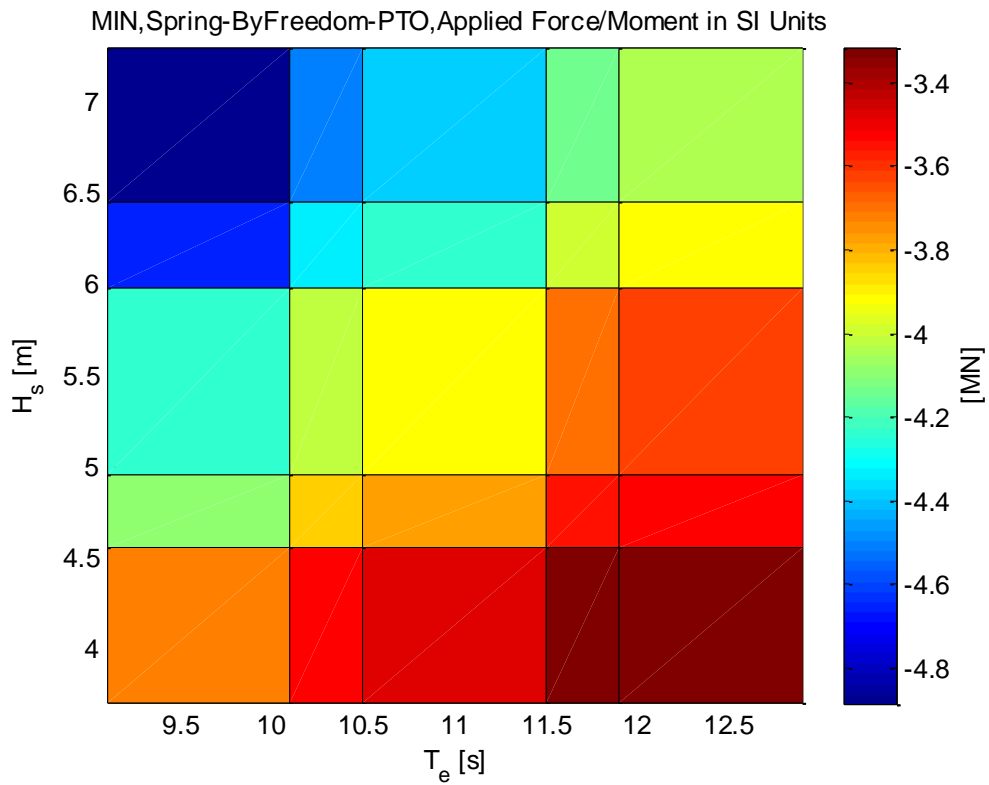


Figure 4-38 Min of PTO applied force for irregular unidirectional extreme waves

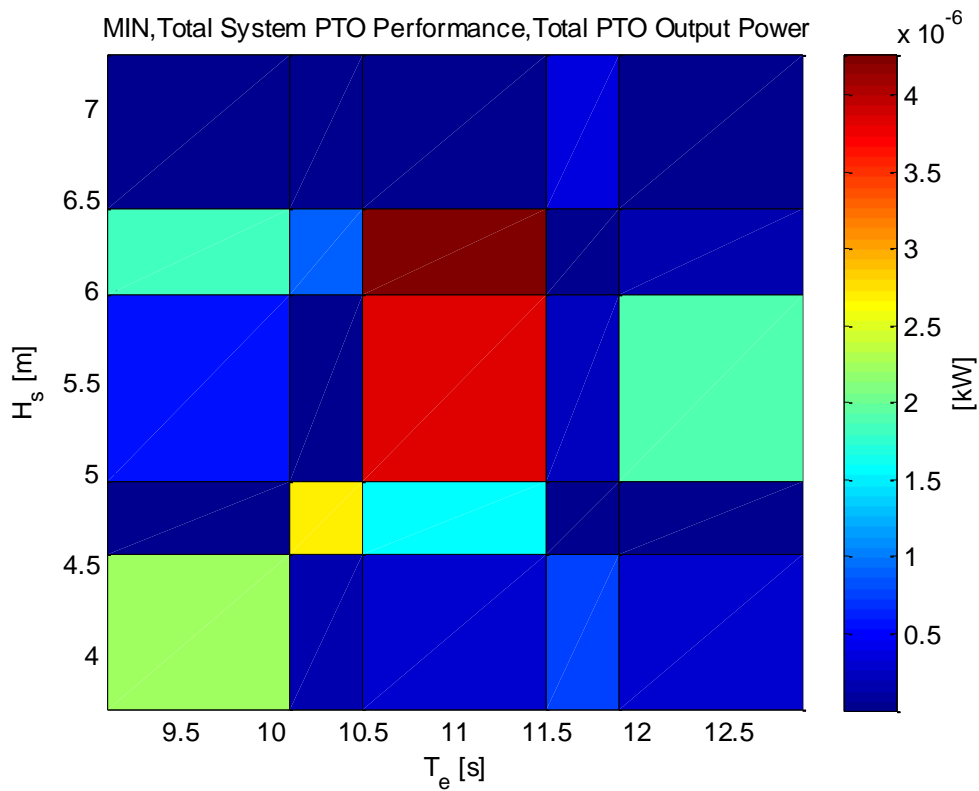


Figure 4-39 Min of PTO power output for irregular unidirectional extreme waves



5 CONCLUSIONS

This report has investigated the motions, performance and PTO loads of a point absorber WEC. The normal and extreme environmental conditions at the WETS location is based on numerical and measured data sets. An extremes analysis was conducted as part of the project in order to derive suitable return values for H_s and the associated energy period.

The WEC model of the point absorber was based on a previous study; however, modifications were made to the water level and the buoy link lengths in order to optimise the performance of the WEC for the WETS location. In addition, an extra degree of freedom was added to the hinges, which in spread sea states, allows global roll and global sway of the device.

The response and force amplitude operators showed that resonant motions occur close to 0.9 and 0.8 rad/s in heave and pitch respectively. The heave motions increased approximately linearly with respect to significant wave height however the pitch motions are nonlinear around the resonant frequency.

Simulations of unidirectional and spread irregular waves has provided a significant range and volume of data for future numerical verification studies. The results of the simulations will be provided to the Customer for comparison to other simulation packages. The binary output files and necessary tools to read the outputs will be provided separately to this technical note, via an agreed medium.

6 REFERENCES

- /1/ Agreement for services and RCUH P.O #Z10027978, 15 April, 2013
- /2/ Amendment No. 1 to the services agreement between the Research Corporation of the University of Hawaii and Garrad Hassan America, Inc, 14th August 2014
- /3/ Email from Luis Vega to Jarett Goldsmith, 23th October 2015
- /4/ Email from Luis Vega to Jarett Goldsmith, 24h October 2015
- /5/ Email from Luis Vega to Jarett Goldsmith, 31th July 2015
- /6/ Email from Luis Vega to Jarett Goldsmith, 11th February 2016
- /7/ WEC Performance Model Verification – Progress Report #1. Hawaii National Marine Renewable Energy Centre – WEC Ocean Testing. 702053-UKBR-T-03-A. 29/01/16
- /8/ Li N, Cheung, K. F. Wave Energy Resource Characterisation at the US Navy Wave Energy Test Site and other Locations in Hawai'i. November 2014. Department of Ocean and Resources Engineering University of Hawai'i.
- /9/ Forristall G, Heideman J, Legget I, Roskam B, Vanderschuren L. Effect of Sampling Variability on Hindcast and Measured Wave Heights, Sep 1996., Journal of Waterwat, Port, Coastal and Ocean Engineering. Vol. 225.
- /10/ Coles, S. An introduction to statistical modelling of extreme values. Springer, 2001.
- /11/ National oceanic and atmospheric administration: national data buoy centre. <http://www.ndbc.noaa.gov/> . Accessed on 01/02/2016.
- /12/ Michell JH, On the highest wave in water (1983). Phil. Mag., 36, 430-435.
- /13/ Ewans, KC, Observations of the directional spectrum of fetch-limited waves (1998). Journal of Physical Oceanography. Vol. 23, page 495-512.
- /14/ Format of Bladed Header files. DNV GL technical note.
- /15/ MathWorks: Software product MATLAB. www.mathworks.com/products/matlab. Accessed on 21/03/2016.

APPENDIX A WAVEDYN OUTPUT FILES

As part of the present study, WaveDyn output files have been provided to HNEI. Appendix A.1 describes the folder structure of the output files provided and Appendix A.2 gives a method for reading the output files to enable a more detailed analysis.

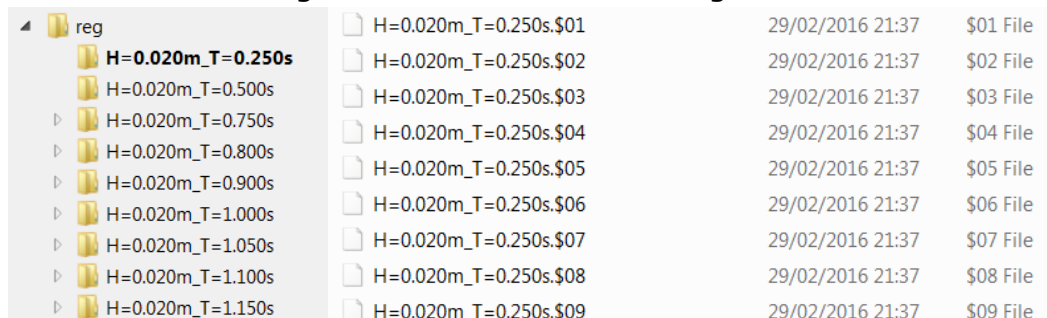
Appendix A.1 Folder structure

The data has been provided in compressed folders. The simulations have been broken down into respective folders labelled using the following convention:

1. Regular waves in folder **reg**
2. Normal wave conditions:
 - a. Unidirectional irregular in folder **uni_normal**
 - b. Spread irregular in folder **spread_normal**
3. Extreme wave conditions:
 - a. Unidirectional irregular in folder **uni_extremes**
 - b. Spread irregular in folder **spread_extremes**

Each folder contains a series of subfolders which each represent a simulated sea state. Each sea state subfolder then contains WaveDyn outputs. An example of the structure of the folder containing regular wave simulations is given in Figure A-1.

Figure A-1 Folder structure of regular wave simulations



Folder Name	File Name	Timestamp	File Type
reg	H=0.020m_T=0.250s.\$01	29/02/2016 21:37	\$01 File
H=0.020m_T=0.250s	H=0.020m_T=0.250s.\$02	29/02/2016 21:37	\$02 File
H=0.020m_T=0.500s	H=0.020m_T=0.250s.\$03	29/02/2016 21:37	\$03 File
H=0.020m_T=0.750s	H=0.020m_T=0.250s.\$04	29/02/2016 21:37	\$04 File
H=0.020m_T=0.800s	H=0.020m_T=0.250s.\$05	29/02/2016 21:37	\$05 File
H=0.020m_T=0.900s	H=0.020m_T=0.250s.\$06	29/02/2016 21:37	\$06 File
H=0.020m_T=1.000s	H=0.020m_T=0.250s.\$07	29/02/2016 21:37	\$07 File
H=0.020m_T=1.050s	H=0.020m_T=0.250s.\$08	29/02/2016 21:37	\$08 File
H=0.020m_T=1.100s	H=0.020m_T=0.250s.\$09	29/02/2016 21:37	\$09 File
H=0.020m_T=1.150s			


Appendix A.2 Reading binary file format

The output files have been provided in a binary file format known as Bladed file format. Bladed file format can be loaded either using the View Results feature in WaveDyn or using a Matlab /15/ p-file called `readBladedOutput.p`. The file can be run using Matlab 2013 or later.

The Bladed file format consists of two files. The first is a header file (`.$xx`) which provides meta-data including the time of the simulation, the variables stored and the format of the data file. The second is the data file (`.$xx`) which contains the time domain outputs of machine or environmental variables written in binary format. The file format is described in more detail in the document /14/.

The p-file takes the following inputs `readBladedOutput(input1, input2, ...)` which are listed in order:

1. A string giving the directory where outputs are contained.
2. A string of the file name
3. A string of the number in the file extension. Note leading zeros must be provided.



The following gives an example of an input to the Matlab command line in order to read the first set of WaveDyn files in the folder shown in Figure A-1.

```
m=readBladedOutput('.\reg\H=0.020m_T=0.0250s\', ' H=0.020m_T=0.0250s ', '01');
```

The output `m` is a structure which provides the simulation time, the data outputs of variables, names of variables read from the file, the units of the variables, etc.



ABOUT DNV GL

Driven by our purpose of safeguarding life, property and the environment, DNV GL enables organizations to advance the safety and sustainability of their business. We provide classification and technical assurance along with software and independent expert advisory services to the maritime, oil and gas, and energy industries. We also provide certification services to customers across a wide range of industries. Operating in more than 100 countries, our 16,000 professionals are dedicated to helping our customers make the world safer, smarter and greener.